2008

Nonlinear State Estimation in Polymer Electrolyte Membrane Fuel Cells

Uma Tumuluri
Cleveland State University

NONLINEAR STATE ESTIMATION IN POLYMER ELECTROLYTE MEMBRANE FUEL CELLS

UMA TUMULURI

Bachelor of Chemical Engineering

Osmania University

April, 2006

Submitted in partial fulfillment of requirements for the degree

MASTER OF SCIENCE IN CHEMICAL ENGINEERING

at the

CLEVELAND STATE UNIVERSITY

December, 2008

This Thesis has been approved for the Department of Chemical and Biomedical Engineering and the College of Graduate Studies by

_____

Thesis Committee Chairperson, Dr. Sridhar Ungarala

_____

Department/Date

_____

Dr. Orhan Talu

_____

Department/Date

_____

Dr. Dhananjai B. Shah

_____

Department/Date

ACKNOWLEDGEMENTS

I would like to take this opportunity to thank my graduate advisor Dr. Sridhar Ungarala, for his time, patience and invaluable guidance throughout my research. He has been a constant source of motivation and inspiration to me.

I would like to thank my thesis committee members, Dr. Orhan Talu and Dr. Dhananjai B. Shah for their time and guidance even in their busy schedules.

My special thanks to Ms. Becky Laird and Ms. Darlene Montogomery for all the help and affection all through these years.

I would like thank my parents and my brother for their love and support. I would like to thank my cousins Mr. Chandra Sekhar Tumuluri and Mrs. Bhargavi Potturi whose moral support meant a lot to me. I thank all my friends for their encouragement and especially my room mates Ms. Gowri K. Potharaju, Ms. Anusha Yerroju, Ms. Sirisha Yerroju for their love and moral support. I would like to thank Mr. Rajmohan Rangarajan , Mr. Anil Singaraju, Mr. Kamal Satya Sai Singaraju and Mr. Mahendranath Potharaju for the friendship and support.

NONLINEAR STATE ESTIMATION IN POLYMER ELECTROLYTE MEMBRANE FUEL CELLS

UMA TUMULURI

ABSTRACT

Research on alternative and renewable energy sources which are amicable to the environment has gained momentum because of the growing concern about the tremendous increase in the concentration of toxic and green house gases and scarcity of the fossil fuels. Among the available renewable sources, fuel cell technology has received a high research attention due to their high efficiency and superior reliability. Among the various fuel cells available, Polymer electrolyte membrane fuel cell is promising source for both stationary and mobile applications because of its high efficiency and low operating temperatures. The performance of the fuel cell depends on the partial pressure of the hydrogen and oxygen, temperature of the stack and membrane humidity. A major obstacle in achieving active control of membrane water content and reactant supply is lack of reliable measurements of partial pressure of the gases and membrane humidity which motivates the use of estimators for estimating the partial pressure of the reactants. This thesis investigates the use nonlinear estimators such as sequential Monte Carlo and unscented Kalman filter to the estimate the partial pressure of hydrogen and oxygen and temperature. The performance of the two filters is studied for cases of poor filter

initialization, plant-model mismatch and multiple load variations by calculating the mean square error. The performance of unscented Kalman filter was better than the sequential Monte Carlo which was not anticipated.

TABLE OF CONTENTS

Page

NOMENCLATURE

A	Active cell area
V_{cell}	Actual cell voltage
c^*_{H2}	Surface concentration of H_2
c^*_{O2}	Surface concentration of O_2
c^*_{H2O}	Surface concentration of H_2O
E^0	Standard state reference potential
E_{thermo}	Thermodynamic cell voltage
F	Faraday constant
ΔF_e	Standard free energy of activation for the reaction
i	Current
K_a	Anode flow constants
K^0	Intrinsic rate constant
l_{mem}	Membrane thickness
N	Number of cells
p'_{H2}	Hydrogen partial pressure
p'_{O2}	Oxygen partial pressure
P_{elec}	Electrical power output
P_k	Error covariance
P_{tank}	Hydrogen inlet pressure

P_{BPR} Oxygen outlet pressure

K_k Kalman gain

K_c Cathode flow constants

Q Process covariance

R Universal gas constant

R Measurement covariance

r_M Membrane resistivity

T Temperature

$T_{cw,in}$ Inlet cooling water temperature

$T_{cw,out}$ Outlet cooling water temperature

T_{amb} Ambient temperature

V_a Anode volume

V_c Cathode volume

V_{sctack} Stack voltage

x_k State vector

y_k Measurement

u_{k-1} Control input at time k-1

A, B, H Transition matrices

Greek Symbols

α_c Transfer coefficient

ω_k Process noise

υ_k Measurement noise

$\zeta_1, \zeta_2, \zeta_3, \zeta_4$ parametric coefficients for activation over potential

λ Adjustable parameter

LIST OF TABLES

Table **Page**

LIST OF FIGURES

Figure **Page**

CHAPTER I

INTRODUCTION

In recent years, there has been a growing concern about limited resources of the fossil fuels and environmental pollution caused by the emission of toxic gases such as CO_2, CH_4, NO_x, SO_x and chlorofluorocarbons, which made the search for alternative energy sources an attractive option. In addition to the available renewable sources such as wind, solar energy etc, fuel cell technology has begun to receive high research attention. It is considered to be a potential replacement for the conventional engines because of its high efficiency and less aggression to the environment thereby reducing the ubiquitous dependence on fossil fuels for power generation.

Fuel cells are electrochemical devices that convert chemical energy present in the fuel directly into electrical energy. The byproducts of this electrochemical reaction are heat and water. In the internal combustion engine, first the fuel energy is converted into thermal energy by the combustion of fuel with oxygen at high temperature. The thermal energy is then converted into mechanical energy. Whereas, in the fuel cells, fuel energy is directly converted into electrical energy. Unlike the internal combustion engines, the fuel cells are not limited by the Carnot efficiency and therefore they are more efficient than the conventional thermal engines. High efficiency, low emission of the toxic gases,

superior reliability are some of the key factors for considering fuel cells as the alternative to conventional internal combustion engines. The automobile industry has played a key role in advancing the fuel cell technology and apart from automobile applications, fuel cell technology is used in telecommunication installations and power generation.

The principle of the fuel cells was discovered by William R. Groove in 1839. By spatially separating the two electrochemical half reactions, the electrons are forced to flow through the external circuit to do useful work before completing the reaction. The electrolyte allows only the ions to pass through while the electrons are forced to flow through external circuit.

1.1 Types of Fuel Cells

Fuel cells are differentiated by the type of electrolyte used for conducting ions. They are

- Polymer electrolyte membrane fuel cell (PEMFC)
- Alkaline fuel cells (AFC)
- Phosphoric acid fuel cell (PAFC)
- Molten carbonate fuel cells (MCFC)
- Solid oxide fuel cells (SOFC)

The underlying electrochemical principle is the same for all the above fuel cells. Fuel is oxidized into electrons and protons at the anode and the oxygen is reduced to oxide species at the cathode. The protons or the oxide ions are transported through the electrolyte and combines with oxide or protons to generate water and power. But they

operate at different temperatures, employ different materials for construction and differ in the fuel tolerance and performance. The operating temperatures, charge carriers, materials employed and the electrolyte used in different fuel cell types are listed in Table I

TABLE I: MAJOR FUEL CELL TYPES

	PEMFC	**AFC**	**PAFC**	**MCFC**	**SOFC**
Electrolyte	Polymer membrane	Liquid KOH (immobilized)	Liquid H_3PO_4 (immobilized)	Molten Carbonate	Ceramic
Charge carrier	H^+	OH^-	H^+	CO_3^{2-}	O^{2-}
Operating temperature	80^{o}C	60-250^{o}C	200^{o}C	650^{o}C	600-1000^{o}C
Catalyst	Platinum	Platinum	Platinum	Nickel	Nickel
Cell components	Carbon based	Carbon based	Carbon based	Stainless steel based	Ceramic based
Fuel compatibility	H_2, methanol	H_2	H_2	H_2, CH_4	H_2, CH_4, CO
Electrical efficiencies	45-55%	45-55%	40-50%	50-55%	50-55%

Fuel cells are also classified as low, intermediate and high temperature fuel cell according to the operating temperatures. Both molten carbonate fuel cells and solid oxide fuel cells are high temperature fuel cells operating around 650^{o}C (MCFC) and 600-1000^{o}C (SOFC).They are highly efficient and internal reforming can be achieved because of the high operating temperatures. The electrolyte used in the molten carbonate fuel cells is

molten mixture of alkali carbonates, lithium carbonate Li_2CO_3 and potassium carbonate K_2CO_3 which is immobilized in $LiAlO_2$ matrix. The charge carriers in the molten carbonate fuel cell are carbonate ions (CO_3^{2-}). Molten carbonate fuel cells can run on hydrogen or simple hydrocarbons such as methane and are not prone to carbon monoxide contamination. Because of the stresses created by the freeze-thaw cycle of the electrolyte during startup and shut down cycles, molten carbonate fuel cells are used in stationary and continuous power generation [1]. Solid oxide fuel cells employ solid ceramic material as an electrolyte. The charge carriers in the solid oxide fuel cells are O^{2-}. It uses nonprecious metal as catalyst and it is fuel flexible. CO poisoning is not an issue and in turn it is used as fuel.

Phosphoric acid fuel cells are the intermediate temperature fuel cells which use liquid phosphoric acid immobilized in SiC matrix as an electrolyte. Protons (H^+) are the charge carriers in phosphoric acid fuel cells. Due to the stresses caused by the free-thaw cycle, phosphoric acid fuel cells are maintained at operating temperature. For optimal performance, phosphoric acid fuel cells are operated at temperatures around 180-210^oC. Phosphoric acid fuel cells are tolerant to the presence of CO_2 in the fuel but they are susceptible to the carbon monoxide and sulfur poisoning as they use platinum catalysts.

Low temperature fuel cells include polymer electrolyte membrane fuel cells (PEMFC), alkaline fuel cells (AFC). Polymer electrolyte membrane fuel cells employ polymer membrane, usually persulfonated polytetrafluoroethylene (Nafion) as an electrolyte. Protons (H^+) are the charge carriers in the polymer electrolyte membrane fuel cells. High power density, fast-start and on-off cycling characteristics and low temperature operation (80^oC) makes the polymer electrolyte membrane fuel cells suitable for portable power

and transport applications. However, they are highly susceptible to carbon monoxide and sulfur contamination. Alkaline fuel cells use aqueous potassium hydroxide electrolyte with hydroxyl ions (OH^-) as charge carriers and depending on the concentration of potassium hydroxide in the electrolyte, they can operate at temperatures between 60-250^oC. Alkaline fuel cells require pure hydrogen and oxygen as they cannot tolerate atmospheric levels of carbon dioxide and this can be partially mitigated by using CO_2 scrubbers and continuously replenishing KOH. However these processes involve additional equipment cost and make it economically not suitable for terrestrial power applications.

Among these fuel cells, polymer electrolyte membrane fuel cell is considered to be a promising substitute of conventional internal combustion engines that can be used in both stationary and mobile applications because of its low operating temperatures and relatively simple design.

1.2 Polymer Electrolyte Membrane Fuel cells

Since the output voltage of a single cell is about 0.6-0.8V which is insufficient for most applications, the fuel cells are stacked together in series to obtain high voltages. A single cell consists of a membrane electrode assembly in which a thin polymer membrane is sandwiched between the two electrodes. Each electrode contains a catalyst layer and a gas diffusion layer. The membrane acts as an electronic insulator, but it is a good conductor of ions. Simple representation of the fuel cell is shown in Figure 1.

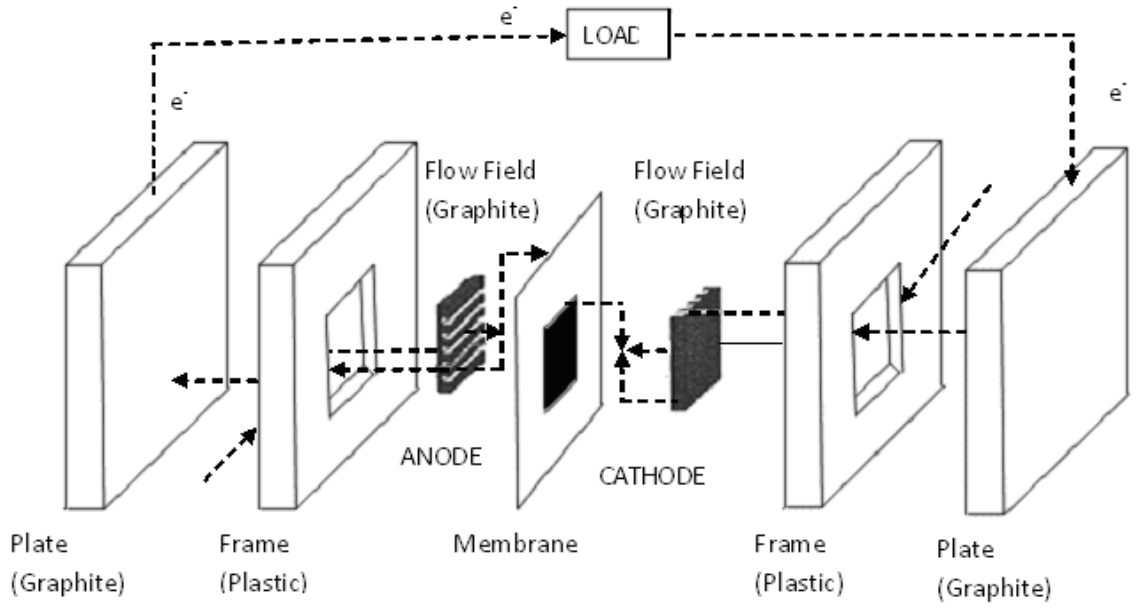

Figure 1: Component description of PEMFC

Fuel (hydrogen) travels from the inlet manifolds to flow fields and diffuses to the catalyst layer through anode. In the catalyst layer, the hydrogen splits into H^+ ions and electrons. The generated hydrogen ions are transported to the cathode interface by the electrolyte membrane while the electrons are forced to flow through the external load towards the cathode, where it combines with oxygen and hydrogen ions to form water molecules and heat [Figure 1]. The electrochemical reaction at anode and cathode can be written as

$$\begin{aligned} &Anode: H_2 \leftrightarrow 2H^+ + 2e^- \\ &Cathode: \frac{1}{2}O_2 + 2H^+ + 2e^- \leftrightarrow H_2O \\ &Overall: H_2 + \frac{1}{2}O2 \leftrightarrow H_2O + Heat \end{aligned} \tag{1.1}$$

The performance of the polymer electrolyte membrane fuel cells is highly dependent on the partial pressure of hydrogen and oxygen, the temperature of the stack and the humidity of the membrane. Inadequate partial pressures of the gases results in voltage drop followed by the damage of membrane. Insufficient supply of the reactants results in the starvation of the cell. Excess water removal causes membrane drying ensuing in the increased ionic resistance and thus decreasing the electrical efficiency which in turn results in further drying of the membrane (hot spots). Conversely, excess water stored in the membrane results in cell flooding. To avoid degradation of voltage and to extend fuel cell stack life, air and fuel flows, pressures of the gases and membrane humidity must be controlled properly.

1.3 Control of Fuel Cells

A major obstacle to the active control of membrane water content and the pressures of gasses is the lack of reliable measurements of membrane humidity and partial pressure of the reactants. High cost and structural sensitivity limits the use of existing sensors in real applications. Difficulties in measuring these variables accurately combined with the importance of these variables accentuate the need of estimator design.

Grujicic et. al. [2] developed a mathematical model for the polymer electrolyte membrane fuel cell system which consists of air and fuel supply sub systems, air and fuel humidifier and a fuel cell stack. The developed model is used to design a feedback control to

maintain the necessary level of oxygen partial pressure in the cathode following the abrupt changes in the stack current demanded by the user.

McKay and Stefanopoulou [3] developed a lumped parameter model for estimating relative humidity of the electrodes. A nonlinear estimator is developed for the estimation of membrane humidity which makes use of the model developed to estimate the electrode humidity, pressure and inlet and outlet temperature at the electrodes. They also designed feedback controller to regulate the excess oxygen ratio during changes in load [4]. Two control problems were discussed in their book. The goal of the first control problem is to regulate the oxygen concentration in the cathode for a high pressure direct hydrogen fuel cell system. The second control problem is multi-input, multi-output control of low pressure partial oxidation based on natural gas fuel processor system. The goal of this control problem is to regulate the catalytic partial oxidation temperature and the hydrogen concentration at anode.

Arcak et al. [5] developed an adaptive scheme to estimate the partial pressure of hydrogen. The adaptive observer is designed by treating the inlet partial pressure as an unknown parameter and by using the voltage injection term. This observer design can be used to estimate the partial pressure of oxygen simultaneously. They also developed estimation scheme for the membrane water content by using the observers designed for the estimation of partial pressures [6]. Initially, the membrane resistance is estimated by calculating the ohmic voltage loss from voltage and current measurements and the voltage model which accounts for other voltage loss terms. The membrane water content is then estimated using the characterizations of the membrane resistance as function of water content. This method also makes use of the observers designed to estimate the

partial pressures of the reactant gases. However, the observer design for the estimation of partial pressure of hydrogen is sensitive to the measurement disturbances at high hydrogen partial pressures. The above estimators are developed for the polymer electrolyte membrane fuel cells.

1.4 Motivation

An active control of feed gas supply is necessary to achieve satisfactory load following performance and simultaneously meeting the dynamic constraints on the supply of reactants. This is possible only when the partial pressure of the gases is known. The information about the partial pressure of the reactants is fed back to design feedback control. However, high cost and sensitivity to the variations in the gas composition limits the use of sensors in the practical applications. This motivates the use of estimators to find the partial pressure of hydrogen and oxygen at anode and cathode respectively. These estimators must be able to incorporate the nonlinear model (as the fuel cell behavior is highly nonlinear) and account for noise in the measurements.

1.5 Scope of the Thesis

The main focus of this thesis is to investigate the use of sequential Monte Carlo filter and unscented Kalman filter to estimate the partial pressure of hydrogen and oxygen and temperature in polymer electrolyte membrane fuel cell.

Sequential Monte Carlo and unscented Kalman filter are recent developments in the field of for the nonlinear state estimation. The main idea of both filters is to represent the probability density functions of state variables with a set of points (samples) and apply an optimization criterion for computing an optimal state estimate. The main difference in these filters is the method of drawing samples. Unscented Kalman filter chooses the samples deterministically which exhibit specific properties. Whereas the samples in sequential Monte Carlo filter are drawn randomly. The mathematical model of the PEM fuel cell used for the simulation study is taken from the reference [1]. This is a generalized model which includes the dynamic features of the electrochemistry of fuel cells, reactant flow and energy balance and can be studied for system design and performance evaluation.

In practical applications, while operating under a variety of load it is quite common for the overall load to fluctuate rapidly because of the switching of the electrical appliances that draw power from the fuel cell system. To simulate the PEM fuel cell during such changes in load, the system model is integrated by implementing step changes in the input current.

The performance of both sequential Monte Carlo filter and unscented Kalman filter is studied for two cases

- Poor filter initialization: The performance i.e., the time taken for the estimates from both the filters to converge to the true states and the mean squared error of

the estimates is analyzed when the filters are initialized with the initial estimates which are far from the true values.

- Plant Model Mismatch: The performance of the filters is analyzed for the case where the system model used in the filters is not accurate enough to represent the true process. A mismatch between the true process and the model is introduced in a few parameters in the model used by the filters.

This thesis discusses the estimation of partial pressure of the reactants and the temperature only, the control of the supply of feed gases is not discussed and left for future work.

1.6 Organization of the Thesis

This thesis is organized as follows. Chapter 2 describes the mathematical model of polymer electrolyte membrane fuel cells. The concepts of electrochemistry of fuel cells, reactant flow and energy balance are discussed in detail in this chapter. Chapter 3 discusses state estimation and various filters used for linear and nonlinear systems. Unscented Kalman filter and sequential Monte Carlo algorithm are discussed in detail in this chapter. Chapter 4 presents the simulation results and the performance of unscented Kalman filter and sequential Monte Carlo is analyzed. Chapter 5 summarizes the thesis and provides direction for the future work.

CHAPTER II

MATHEMATICAL MODEL FOR FUEL CELLS

The efficiency and robustness of the fuel cell technology is dependent on understanding, predicting, monitoring and controlling the fuel cell system under wide operating range and different environmental conditions. However this requires a thorough understanding of many physical, electrochemical, thermal and fluid dynamic issues. A number of mathematical models of fuel cells are available in the literature.

Carcadea et al. [7] developed a three dimensional model where the flow and mass transfer patterns were investigated in order to understand the fuel cell operation and to improve its performance. Springer et al. [8] developed an isothermal one dimensional steady state model which concentrates on water transport mechanisms. The membrane resistance and concentration of oxygen are obtained by solving the proposed water balance equations which are in turn used to determine the cathode potential and V-I curve of the fuel cell.

Rowe and Li [9] developed a one dimensional nonisothermal model to investigate the effects of design and operating conditions on the fuel cell performance, thermal response and water management.

Baschuk et al. [10] developed a model based on the hydraulic network approach. In the model, the pressure and mass flow distributions of the fuel and oxidant within the stack are determined by treating the stack manifold and gas channels as a pipe network. Using these distributions as input parameters, the output voltage of the single cells is determined with the steady state isothermal model.

A nonlinear model was developed by Pukrushpan et al. [4] which incorporates the dynamic model of the subsystems that are useful for the control study of fuel cell system. This model is used to design a feedback controller that regulates the excess oxygen ratio in the cathode during step changes in fuel cell current.

Amphlett et al. [11] developed steady state parametric model which gives cell voltage for a given set of operating conditions such as concentration of the reactant gases, pressure and current. This model is developed using mass transfer properties, thermodynamic equilibrium potentials and over voltages. Parametric equations were obtained using linear regression analysis to determine the over voltages i.e., the activation over voltage and ohmic over voltage [12]. The transient model was also developed by the same authors, which predicts the cell voltage and temperature as function of time when perturbations such as step change in operating current or system shut down was imposed in the system [13]. Khan et al. developed an empirical model where the general steady state model developed by Mann et al. [14] is extended for dynamic electrochemical analysis [15]. The empirical model developed by Khan et al. was used as the system model in this thesis.

Model Formulation

As the fuel cell behavior is highly non linear and depends on a range of factors, a set of assumptions were considered to simplify the analysis [1]. They are

- The membrane is fully saturated with water.
- The partial pressure of the reactants depends on the inlet flow rates and their consumption and the variations in partial pressures affect the system.
- The system is isothermal.
- The total pressure inside the stack is uniform, whereas variations in the partial pressure of the reactants affect the system.

The fuel cell model consists of three sub models, namely, the electrochemical model, the thermal model and the reactant flow model as shown in Figure 2 anode flow and cathode flow models calculate the partial pressure of hydrogen (p'_{H2}) and oxygen (p'_{O2}) by employing the mass balance equations. They also take the hydrogen tank pressure, air flow rate and stack current as the inputs. The thermal model calculates the stack temperature (T' in ^{o}C) by employing the energy balance equations. The inputs of this model are stack current (i) and the calculated stack voltage (V_{stack}) from the electrochemical model. The concepts of electrochemistry of the fuel cell are discussed in the electrochemical model. This model calculates the voltage of the cell (V_{cell}) by taking the partial pressure of hydrogen and oxygen from the anode and cathode flow models, temperature (T in ^{o}K) from the thermal model and stack current as inputs. The voltage of

the single cell is multiplied with the total number of fuel cells (*N*) connected in series to get the stack voltage

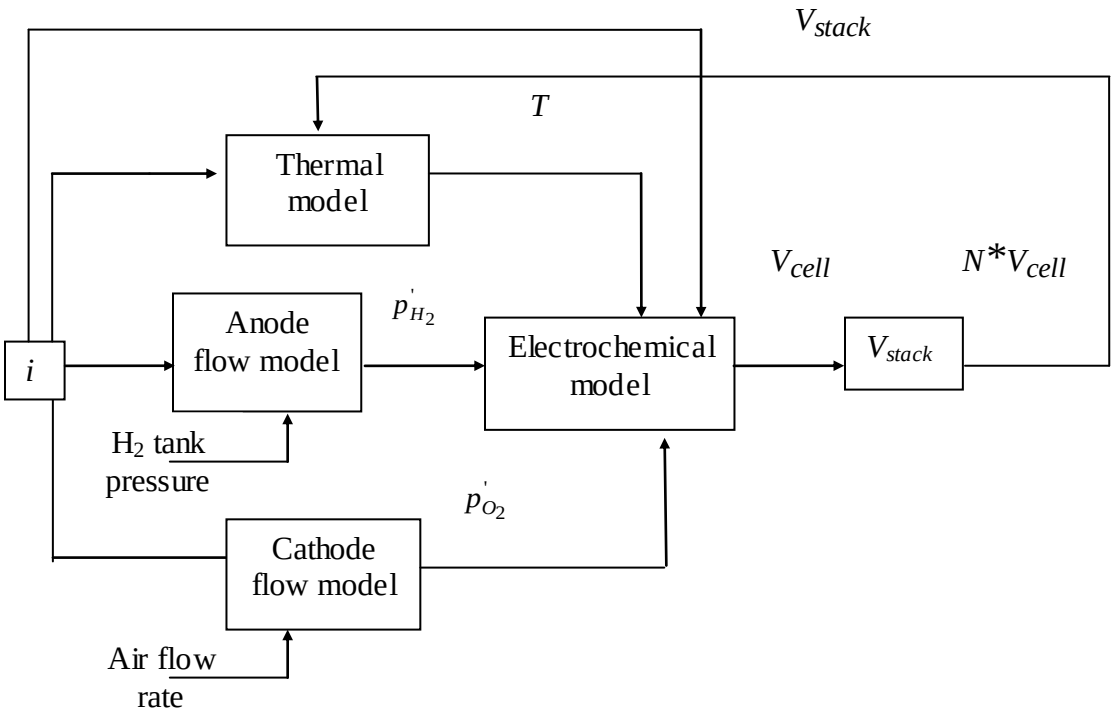

Figure 2: Fuel cell system sub models

2.1 Electrochemical Model

The output voltage (V_{cell}) of single cell is a function of stack current, temperature, partial pressure of reactant, and membrane humidity. It can be defined as

$$V_{cell} = E_{thermo} + \eta_{act} + \eta_{ohmic} \tag{2.1}$$

Where E_{thermo} is the thermodynamic equilibrium potential or open circuit voltage and η_{act} η_{ohmic} are activation over voltage and ohmic over voltage respectively. The over voltage terms are negative and they represent the voltage drop.

2.1.1 Open Circuit Voltage

Thermodynamic potential or the reversible cell voltage is the maximum voltage attained from a fuel cell at thermodynamic equilibrium. It can be defined by the Nernst equation as

$$E_{thermo} = E^0 + \frac{RT}{nF}\ln\left[p'_{H2}\left(p'_{O2}\right)^{0.5}\right] \tag{2.2}$$

Where E^0 is the standard state reference potential (298.15 K and 1 atm) at unit activity and its variation with the temperature can expressed as

$$E_{thermo} = 1.229 - 0.85*10^{-3}(T - 298.15) + \frac{RT}{nF}\ln\left[p'_{H2}\left(p'_{O2}\right)^{0.5}\right] \tag{2.3}$$

where p'_{H_2} and p'_{O_2} are partial pressure of hydrogen and oxygen respectively, T is the stack temperature (^{o}K), R is the universal gas constant (8.314 J/mole K), F is the Faraday constant (96,485 C/mole) and n represents the number of moles of electrons transferred. The output voltage is never equal to the thermodynamic potential because of irreversible losses.

2.1.2 Activation Over Voltage

A part of the voltage is lost in driving the chemical reaction at the electrodes. This lost voltage is known as activation over voltage (η_{act}). It occurs at both anode and cathode. Since the hydrogen oxidation is faster than oxygen reduction, the activation over voltage at cathode is more predominant. Activation over voltage can be represented by a parametric equation as [11]

$$\eta_{act} = \xi_1 + \xi_2 T + \xi_3 T\left[\ln\left(c^*_{O2}\right)\right] + \xi_4 T[\ln(i)] \tag{2.4}$$

The values of the parametric coefficients ζ_1, ζ_2, ζ_3, ζ_4 are determined using linear regression analysis by Amphlett et al. [8]. They are

$$\begin{aligned} \xi_1 &= -0.948 \\ \xi_2 &= 0.00286 + 0.002\ln(A) + 4.3*10^{-5}\ln\left(c^*_{H2}\right) \\ \xi_3 &= 7.6*10^{-5} \\ \xi_4 &= -1.93*10^{-4} \end{aligned} \tag{2.5}$$

where c^*_{H2} and c^*_{O2} are concentration of hydrogen, oxygen respectively at the reaction site.

The effective concentration of hydrogen and oxygen at the electrode-membrane interface can be obtained from Henry's law equation of the form [1] [7]

$$c^*_{H_2} = p'_{H_2} 9.174*10^{-7}\exp\left(\frac{-77}{T}\right) \tag{2.6}$$

$$c^*_{O_2} = p'_{O_2} 1.97*10^{-7}\exp\left(\frac{498}{T}\right) \tag{2.7}$$

2.1.3 Ohmic Over Voltage

The voltage which is lost due to the resistance to the flow of electrons through the electrodes and various interconnections and resistance to the flow of ions through the electrolyte is known as ohmic over voltage (η_{ohmic}). It can be written as

$$\eta_{ohmic} = -iR = -i\left(R_{electronic} + R_{ionic}\right) \tag{2.8}$$

The resistance to the flow ions (R_{ionic}) is predominant and hence its contribution to ohmic over voltage is very significant than the resistance to the flow of electrons ($R_{electronic}$). The ionic resistance is a function of the membrane water content which in turn is a function of temperature and current. The ionic resistance can be expressed as

$$R_{ionic} = \frac{r_M l_{mem}}{A} \tag{2.9}$$

where l_{mem} is the membrane thickness (178 μm), A is the active cell area (232 cm^2) and r_M is the membrane resistivity.

The membrane resistivity is a function of type and characteristics of membrane, temperature, water content and current density. The analytical expression for the membrane resistivity was proposed by Amphlett et al. [13].

$$r_M = \frac{181.6\left[1 + 0.03\left(\frac{i}{A}\right) + 0.062\left(\frac{T}{303}\right)^2\left(\frac{i}{A}\right)^{2.5}\right]}{\left[\lambda - 0.634 - 3\left(\frac{i}{A}\right)\right]\exp\left[4.18\left(\frac{T-303}{T}\right)\right]} \tag{2.10}$$

where, the term $\frac{181.6}{\lambda - 0.634 - 3\left(\frac{i}{A}\right)}$ is the membrane specific resistivity at zero current and 30^{o}C temperature. The exponential term is the temperature correction term if the temperature is other than 30^{o}C and the reduction of *3(i/A)* from λ represents empirical correction to the specific resistivity. The term λ is considered as an adjustable parameter which depends on membrane humidity and stoichiometric ratio of anode feed gas. Its value can be in between 10 to 23.

For *N* number of cells connected in series, the stack voltage is obtained by multiplication of cell voltage with the number of cells.

$$V_{stack} = N * V_{cell} \tag{2.11}$$

2.2 Thermal Model

The performance of the fuel cell stack is highly dependent on the thermal management in the stack. Increase in the load current is associated with increase in power dissipated followed by the elevation in the stack temperature. High temperature in the stack results in the dehydration of membrane which in turn reduces the output voltage. Unlike the electrochemical model, which is conducted for a single cell, the thermal modeling is conducted for the entire stack.

The total energy delivered by the inlet hydrogen into the stack is used in four different ways. They are consumption by electrical load, heat removal by the coolant, heat loss at

the surface, and absorption by the stack. The system temperature can be related to the heat absorbed as

$$C_t \frac{dT'}{dt} = \dot{Q}_{stack} \tag{2.12}$$

where C_t is thermal capacitance (17.9 KJ $^oC^{-1}$) and T' is the stack temperature (^oC).

From the energy balance, the rate of heat absorption $\dot{Q}_{stack}$ can be written as

$$C_t \frac{dT'}{dt} = P_{tot} - P_{elec} - \dot{Q}_{cool} - \dot{Q}_{loss} \tag{2.13}$$

The total power delivered into the stack P_{tot} is proportional to the hydrogen consumed which in turn depends on the stack current and total number of cell in the stack.

$$P_{tot} = \frac{Ni}{2F} \Delta H \tag{2.14}$$

Where, ΔH is the enthalpy of combustion for hydrogen.

The electrical output P_{elec} is the product of stack voltage and current.

$$P_{elec} = V_{stack} i \tag{2.15}$$

The rate of heat removal by cooling water is related to the surface area of heat exchanger and the log mean difference between the inlet and outlet cooling water.

$$\dot{Q}_{cool} = UA_{HX} \frac{\left(T' - T_{cw,in}\right) - \left(T' - T_{cw,out}\right)}{\ln\left[\left(T' - T_{cw,in}\right) / \left(T' - T_{cw,out}\right)\right]} \tag{2.16}$$

where, UA_{HX} is the measure of exchanger size, $T_{cw,in}$ and $T_{cw,out}$ are the inlet and outlet cooling water temperatures. UA_{HX} can be determined by the empirical formula as

$$UA_{HX} = h_{cond} + h_{conv} i \tag{2.17}$$

where, as h_{cond} and h_{conv} are the parameters that conduction and convection properties of the heat exchangers. The heat lost by the stack surface $\dot{Q}_{loss}$ is proportional to the temperature of the stack and the ambient temperature.

$$\dot{Q}_{loss} = \frac{T' - T_{amb}}{R_t} \tag{2.18}$$

where T_{amb} is the ambient temperature (25 ^{o}C) and R_t is thermal resistance of the stack (0.115 ^{o}C W^{-1}).

2.3 Reactant Flow Model

The effective partial pressure of the hydrogen and oxygen are determined by the flow rate of reactants at both the electrodes. The reactant partial pressure is determined by applying mass balance and ideal gas law. The partial pressure of hydrogen at the anode is determined as

$$\frac{V_a}{RT}\frac{dp'_{H2}}{dt} = \dot{m}_{H2,in} - \dot{m}_{H2,out} - \dot{m}_{H2,used} \tag{2.19}$$

$\dot{m}_{H2,in}$ and $\dot{m}_{H2,out}$ are the inlet and outlet hydrogen flow rates respectively, V_a is the anode volume (0.005 m^3), $\dot{m}_{H2,used}$ is amount of hydrogen used which is proportional to number of cells and stack current. The above equation can be still modified as

$$\frac{V_a}{RT}\frac{dp'_{H2}}{dt} = \dot{m}_{H2,in} - \dot{m}_{H2,out} - \frac{Ni}{2F} \tag{2.20}$$

Similarly the partial pressure of oxygen at the cathode is determined as

$$\frac{V_c}{RT}\frac{dp'_{O2}}{dt} = \dot{m}_{O2,in} - \dot{m}_{O2,out} - \dot{m}_{O2,used} \tag{2.21}$$

where, $\dot{m}_{O2,in}$ and $\dot{m}_{O2,out}$ are the inlet and outlet flow rates of oxygen at the cathode, V_c is cathode volume (0.01 m^3), $\dot{m}_{O2,used}$ is the amount of oxygen consumed which depends on the number of cells and stack current.

$$\frac{V_c}{RT}\frac{dp'_{O2}}{dt} = \dot{m}_{O2,in} - \dot{m}_{O2,out} - \frac{Ni}{4F} \tag{2.22}$$

The outlet flow rates of the reactants can be related to the partial pressure and down stream pressure as

$$\dot{m}_{H2,out} = K_a\left(p'_{H2} - P_{tank}\right) \tag{2.23}$$

$$\dot{m}_{O2,out} = K_c\left(P'_{O2} - P_{BPR}\right) \tag{2.24}$$

Where K_a (0.065 mol $s^{-1}atm^{-1}$) and K_c (0.065 mol $s^{-1}atm^{-1}$) are flow constants for anode and cathode respectively, P_{tank} and P_{BPR} are hydrogen inlet pressure (3 atm) and oxygen

outlet pressure (3 atm) respectively. The inlet hydrogen pressure is assumed to be maintained at constant pressure of 3 atm. The above equations give the partial pressure of the reactants at any given time for a given inlet low rates, temperature and current.

2.4 Matlab Implementation

All the three sub models were coupled together and simulated in Matlab to calculate the output voltage for changes in the load current [4,15] Originally, this mathematical model was simulated in Simulink but it is recoded in the Matlab for this work as it involves the implementation of filters. These models are simulated with ODE23tb solver and simulated for 4000 seconds and the voltage is sampled every second.

CHAPTER III

STATE ESTIMATION

The main goal of any industrial process is to obtain an end product with lowest possible cost and simultaneously satisfy the product quality constraints. Often, these processes are accompanied with uncertainties such as uncertainty in measurements and noise sources or unknown disturbances acting on the system. Reliable information about the state variables and operating parameters must be available for control and optimization of process. State estimation plays a vital role in the reconstruction of the important state variable which is inaccessible.

In general, the estimation can be formulated as follows. The current state x_k is determined using the available measurements $y_{1:k}$ and the initial guess x_0 in an optimal and recursive manner. In the Bayesian approach, measured or unmeasured states are estimated by propagating the probability density functions of the states over time and by imposing the optimization criterion such as minimum mean squares error or maximum a posterior estimate [16]. The discrete-time dynamic process model can be formulated as

$$\begin{aligned} x_k &= f\left(x_{k-1}, u_{k-1}, \omega_{k-1}\right) \\ y_k &= h\left(x_k, \upsilon_k\right) \end{aligned} \tag{3.1}$$

Where: $x_k \in \Re^n$ is the state vector, $f_k : \Re^n \times \Re^n \to \Re^n$ is the system equation and $y_k \in \Re^n$ are measurements which are related to the state vector through the measurement equation $h_k : \Re^{n_x} \times \Re^{n_\upsilon} \to \Re^{n_y}$ .The system noise $\omega_k \in \Re^{n_\omega}$ represents the disturbance in the system and the inaccuracy in measuring systems is represented by the measurement noise $\upsilon_k \in \Re^n$. Q and R represent noise covariance matrices

For linear systems, the probability density functions can be assumed to be Gaussian which is characterized by its mean and covariance. Kalman filter which relies on the mean and variance of the states is widely used for linear systems. However, the Kalman filter can be applied for nonlinear systems by assuming the process to be linear. If the process is highly nonlinear, then the linear assumption does not yield accurate results. In such cases, the Kalman filter can be applied in the form of extended Kalman filter where the nonlinear states are linearized using Taylor series expansion. This requires calculation of Jacobian matrices which can be difficult and error-prone for some systems. Other state estimators which are developed for nonlinear systems include unscented Kalman filter [17, 18, 1919, Bayesian estimation [16, 20], moving horizon estimation and sequential Monte Carlo [21, 22]. In general, any recursive estimation can be executed in two stages at any time instant.

- Prediction: The next state is predicted given the previous estimate using system model.
- Update: The current state of the system is estimated given the current measurement.

3.1 Kalman Filter

Kalman filter is optimal if the system is linear. Kalman filter is executed in two steps, prediction (time update equations) where *a priori* estimates for the next time step are calculated using the current state and error covariance and correction (measurement update equations) where an improved *a posteriori* estimate is obtained by incorporating new measurement into priori estimates. In the matrix form the linear process model is represented as

$$\begin{aligned} x_k &= Ax_{k-1} + Bu_{k-1} + \omega_{k-1} \\ y_k &= Hx_k + \upsilon_k \end{aligned} \tag{3.2}$$

A, *B*, *H* are the transition matrices for the system model and measurement.

The algorithm for the execution of time update and measurement update equations in the Kalman filters is shown in Figure 3

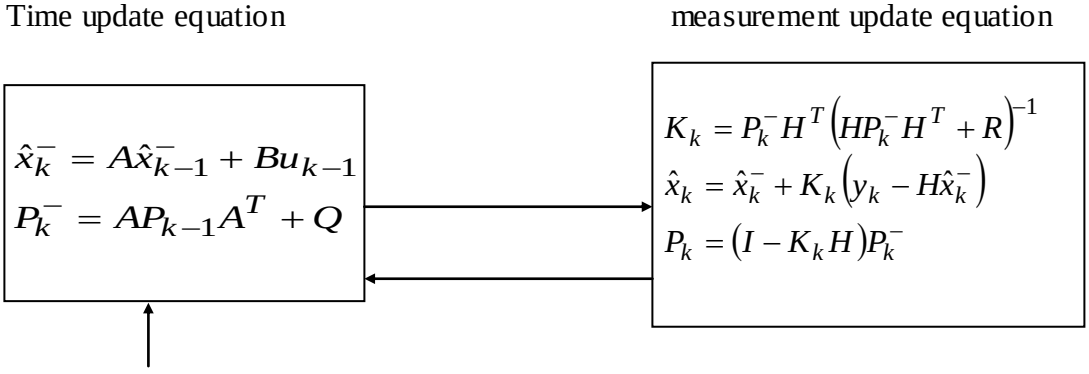

Figure 3: Recursive algorithm for Kalman filter

Where $\hat{x}_k^-$ is *a priori* state estimate at time step *k* given the knowledge of the process prior up to step *k*. $\hat{x}_k$ is *a posteriori* state estimate at time step *k* give the measurement. P_k^- is the *a priori* estimate error covariance, P_k is *a posteriori* estimate error covariance and K_k is the Kalman gain. *R* is measurement noise covariance and *Q* is process noise covariance.

3.2 Extended Kalman Filter

For nonlinear systems, the Kalman filter is applied in the form of extended Kalman filter where the nonlinear states are linearized using Taylor series expansion. This requires the calculation of Jacobian and Hessian (for higher order Kalman filters) matrices. The time and measurement update equations of the extended Kalman filters for nonlinear system which can be represented as above (equation 3.2) can be written as

EKF time update equation

$$\hat{x}_k^- = f(\hat{x}_{k-1}, u_{k-1}, 0) \tag{3.4}$$

$$P_k^- = A_k P_{k-1} A_k^T + W_k Q_{k-1} W_k^T \tag{3.5}$$

EKF measurement update equations

$$K_k = P_k^- H_k^T (H_k P_k^- H_k^T + V_k R_k V_k^T)^{-1} \tag{3.5}$$

$$\hat{x}_k = \hat{x}_k^- + K_k \left(y_k - h\left(\hat{x}_k^-, 0\right)\right) \tag{3.6}$$

$$P_k = (I - K_k H_k) P_k^- \tag{3.7}$$

H_k and V_k are measurement Jacobians at time step k whereas A_k and W_k are process model Jacobians at time k.

$$\begin{aligned} A &= \frac{\partial f}{\partial x}\left(\hat{x}_{k-1}, u_{k-1}, 0\right) \\ W &= \frac{\partial f}{\partial \omega}\left(\hat{x}_{k-1}, u_{k-1}, 0\right) \\ H &= \frac{\partial h}{\partial x}\left(\hat{x}_k^-, 0\right) \\ V &= \frac{\partial h}{\partial \upsilon}\left(\hat{x}_k^-, 0\right) \end{aligned} \tag{3.8}$$

Extended Kalman filter is simple and powerful tool for the estimation of nonlinear states. However it can lead to error since it involves the calculation of Jacobian matrices.

3.3 Unscented Kalman Filter

As mentioned previously, extended Kalman filters are widely used for the nonlinear systems where the nonlinear states are linearized and the calculated Jacobian matrices are substituted in the Kalman filter equations. However it has some drawbacks.

- Linearization can undermine the performance of the filter if the error propagation is not approximated well by the linearized function.
- Linearization is possible only for the systems for which the Jacobian exists and also calculation of Jacobian or the Hessian matrices (for higher order filters) is difficult and can lead to computational errors which may reduce the performance of the filters.

3.3.1 Unscented transform: principle and algorithm

'The main idea of unscented transformation is based on the intuition that it is easier to approximate a probability distribution than to approximate an arbitrary nonlinear function or transformation' (source [18, 19]). The principle of unscented transform is illustrated in Figure 4

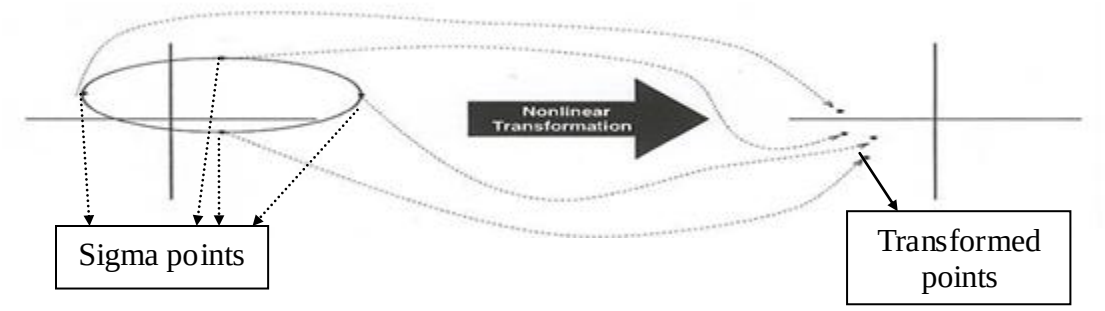

Figure 4: Principle of unscented Kalman filter [18]

A set of sigma points (sample points) with the mean $\bar{x}$ and covariance P_{xx} are chosen and nonlinear function is applied to these sigma points which results in transformed points. The statistics of the transformed sigma points gives the estimate of transformed mean and covariance. It differs with the Monte Carlo method by drawing the samples deterministically which exhibits certain specific properties rather than choosing the samples randomly, thereby capturing the higher-order information about the distribution with less number of points.

For a given mean vector $\bar{x}$ and the covariance P_{xx} of the n dimensional vector x, a set of $2n+1$ sigma points can be deterministically computed as

$$
\begin{aligned}
x_0 &= \bar{x} & W_0 &= \frac{\kappa}{(n+\lambda)} & i &= 0 \\
x_i &= \bar{x} + \left(\sqrt{(n+\lambda)P_{xx}}\ \right)_i & W_i &= \frac{1}{2(n+\lambda)} & i &= 1,....,2n \\
x_{i+n} &= \bar{x} - \left(\sqrt{(n+\lambda)P_{xx}}\right)_i & W_{i+n} &= \frac{1}{2(n+\lambda)} & i &= 1,....,2n
\end{aligned} \tag{3.7}
$$

where, $\left(\sqrt{(n+\lambda)P_{xx}}\ \right)_i$ is the i[th] column of the matrix square root of $(n+\lambda)P_{xx}$ and W_i is its associated weight. $\lambda = \alpha^2(n+\kappa) - n$ is the scaling parameter where as α, κ are tuning parameters. A detailed discussion about the selection of sigma points can be found in [17].

For the mean and covariance to be unbiased, the weights associated with sigma points must satisfy the following condition

$$\sum_{i=0}^{n} W_i = 1 \tag{3.8}$$

With those sigma points, the transformed mean $\bar{y}$ and covariance P_{yy} can be calculated as

- Each sigma point is propagated through the given function to get the transformed sigma points

$$y_i = h(x_i) \qquad i=0,\ldots,\ 2n \tag{3.9}$$

- The weighted average of the transformed points gives the mean $\bar{y}$ and weighted outer product gives the covariance P_{yy} of transformed sigma points

$$\bar{y} \approx \sum_{i=0}^{2n} W_i y_i$$
$$P_{yy} \approx \sum_{i=0}^{2n} W_i (y_i - \bar{y})(y_i - \bar{y})^T \tag{3.10}$$

- The weighted product of original and transformed points gives the cross covariance

$$P_{xy} \approx \sum_{i=0}^{2n} W_i (x_i - \bar{x})(y_i - \bar{y})^T \tag{3.11}$$

3.3.2 Application of unscented transform to Kalman filter

The following algorithm represents the application of unscented transform to nonlinear state estimation.

- The set of sigma points is determined by applying the sigma point selection algorithm. The transformed sigma points are given by propagating each point through the process model.

$$\hat{x}_{k,i} = f(x_{k-1,i}, u) \tag{3.12}$$

- The predicted mean $\bar{x}_k$ and covariance P_{xx} are calculated as

$$\bar{x}_k = \sum_{i=0}^{2n} W_i \hat{x}_{k,i}$$
$$\bar{P}_{xx} \approx \sum_{i=0}^{2n} W_i (x_{k,i} - \bar{x}_k)(x_{k,i} - \bar{x}_k)^T + Q_k \tag{3.13}$$

- The predicted points are propagated through the measurement model

$$\hat{y}_{k,i} = h(\hat{x}_{k,i}) \tag{3.14}$$

- Predicted mean $\bar{y}_{k,i}$ and covariance P_{yy} of measurement and cross covariance P_{xy} of the state and measurement are determined as

$$\begin{aligned} \bar{y}_{k,i} &\approx \sum_{i=0}^{2n} W_i \hat{y}_i \\ \bar{P}_{yy} &\approx \sum_{i=0}^{2n} W_i \left(y_{k,i} - \bar{y}_k\right)\left(y_{k,i} - \bar{y}_k\right)^T + R_k \\ \bar{P}_{xy} &\approx \sum_{i=0}^{2n} W_i \left(x_{k,i} - \bar{x}_k\right)\left(y_{k,i} - \bar{y}_k\right)^T \end{aligned} \tag{3.15}$$

- The state estimate and covariance are updated using filter gain K_k.

$$\begin{aligned} K_k &= P_{xy} P_{yy}^{-1} \\ x_k &= \bar{x}_k + K_k\left(y_k - \bar{y}_k\right) \\ P_{xx} &= \bar{P}_{xx} - K_k \bar{P}_{yy} K_k^T \end{aligned} \tag{3.16}$$

Thus by eliminating the calculation of Jacobian and Hessian matrices for linearization of the nonlinear systems, the unscented Kalman filter can estimate the states more accurately than the extended Kalman filter.

3.4 Sequential Monte Carlo Filter

Sequential Monte Carlo, also known as particle filters are being widely used for non linear state estimation. These are recursive algorithms and they are based Bayesian theory. The main idea of this estimation is to represent the probability density functions of any shape with a set of random samples associated with the weights. As the number of samples increases, the estimate approaches the true value [19].

3.4.1 Bayesian estimation

Bayesian estimation provides a rigorous approach for estimating the probability distribution of the unknown state variables of the system by considering the variables to be stochastic. The distribution of the state variables to be estimated, *x*, given the measurements, *y*, can be written using the Bayes rule as

$$p(x|y) = \frac{p(y|x)p(x)}{p(y)} \tag{3.17}$$

The prior knowledge about the unknown variables is represented by $p(x)$ and the likelihood $p(y|x)$ represents the information contained in the current measurement. The evidence provided by the current measurement which is also a normalizing constant is represented by $p(y)$. For recursive estimation, the posterior $p(x_k|y_{1:k})$ is calculated using the prior $p(x_k|y_{1:k-1})$ along with the current information $p(y_k|x_k)$ as

$$p(x_k|y_{1:k}) = \frac{p(y_k|x_k)p(x_k|y_{1:k-1})}{p(y_k|y_{1:k-1})} \tag{3.18}$$

3.4.2 Sequential Monte Carlo

For a set of samples $\{x_k^i, q_k^i\}_{i=1}^N$, where $\{x^i, i = 1,...N\}$ is a set of *N* number of samples for each state variable with the associated weights as $\{q^i, i = 1,..., N\}$, the posterior can be written as

$$p(x_k|y_{1:k}) = \sum_{i=1}^{N} q_k^i \delta(x_k - x_k^i) \tag{3.19}$$

Importance sampling principle is used to determine the weights. The algorithm for importance sampling can be illustrated as follows. For the probability density *p(x)* which can be approximated by a set of samples $\{x^i, i = 1,...N\}$ with the weights q^i

$$p(x) = \sum_{i=1}^{N} q^i \delta(x - x^i) \tag{3.20}$$

The expectations based on sequential Monte Carlo can be written as

$$E[f(x)] = \int f(x)p(x)dx \tag{3.21}$$

$$E[f(x)] \approx \frac{1}{N} \sum_{i=1}^{N} f[x^i] q^i \tag{3.22}$$

Generating samples distributed as any probability distribution may not be easy. Let $\pi(x)$ be a function from which the samples can be easily drawn to represent the distribution. Above equation (3.23) is reformulated as

$$E[f(x)] = \int f(x)p(x)\,dx \tag{3.23}$$

$$= \int f(x)\frac{p(x)}{\pi(x)}\pi(x)dx \tag{3.24}$$

$$\approx \frac{1}{N} \sum_{i=1}^{N} f(x^i)\frac{p[x^i]}{\pi[x^i]} \tag{3.25}$$

From the above equations (3.22 and 3.23) associated weights of the samples q^i can be written as

$$q^i = \frac{1}{N}\frac{p(x^i)}{\pi(x^i)} \tag{3.26}$$

x^i are the samples drawn from the distribution $\pi(x)$ instead of $p(x)$. $\pi(x)$ is known as importance density. The weights in the equation 3.19 can be written as

$$q^i = \frac{p(x_k^i|y_{1:k})}{\pi(x_k^i|y_{1:k})} \tag{3.27}$$

Importance density function for the recursive estimation can be written as

$$\pi(x|y_{1:k}) = \pi(x_k|x_{k-1}, y_{1:k})\pi(x_{k-1}|y_{1:k-1}) \tag{3.28}$$

Based on Bayesian rule, the probability density function of posterior can be written as

$$p(x_k|y_{1:k}) = \frac{p(y_k|x_k, y_{1:k-1})p(x_k|y_{1:k-1})}{p(y_k|y_{1:k-1})} \tag{3.29}$$

$$= \frac{p(y_k|x_k, y_{1:k-1})p(x_k|x_{k-1}, y_{1:k-1})}{p(y_k|y_{1:k-1})}p(x_{k-1}|y_{1:k-1}) \tag{3.30}$$

$$= \frac{p(y_k|x_k)p(x_k|x_{k-1})}{p(y_k|y_{1:k-1})}p(x_{k-1}|y_{1:k-1}) \tag{3.31}$$

$$\propto p(y_k|x_k)p(x_k|x_{k-1})p(x_{k-1}|y_{1:k-1}) \tag{3.32}$$

Substituting equations 3.30 and 3.26 in equation 3.25

$$q^i \propto \frac{p(y_k|x_k^i)p(x_k^i|x_{k-1}^i)p(x_{k-1}^i|y_{1:k-1})}{\pi(x_k^i|x_{k-1}^i, y_{1:k})\pi(x_{k-1}^i|y_{1:k-1})} \tag{3.33}$$

$$\propto q_{k-1}^i \frac{p(y_k|x_k^i)p(x_k^i|x_{k-1}^i)}{\pi(x_k^i|x_{k-1}^i, y_k)} \tag{3.34}$$

The posterior probability density function (equation 3.19) can be rewritten as

$$p(x_k|y_k) \approx \sum_{i=1}^{N} q_k^i \delta(x_k - x_k^i) \tag{3.35}$$

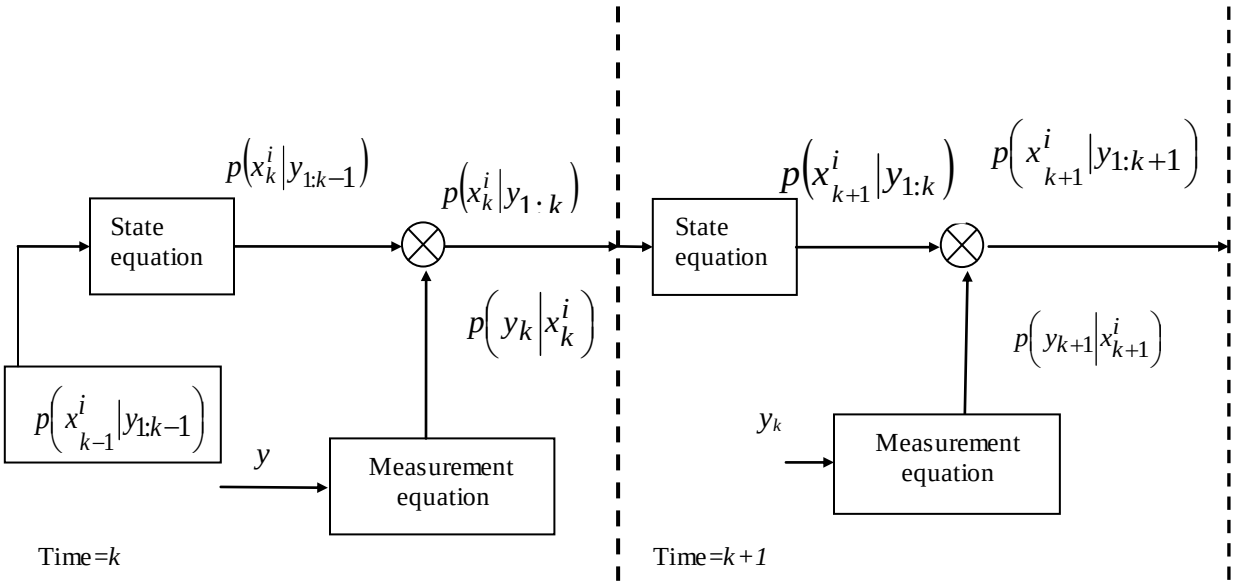

Figure 5: Recursive algorithm for SMC [20]

The recursive algorithm of sequential Monte Carlo filter (Figure 5) for the above nonlinear system model (equation 3.3) can be summarized as

- Initialize: N Random samples are distributed according to the known posterior $p(x_{k-1}^i|y_{1:k-1})$.
- Predict: Each sample is passed through the state equation along with the samples drawn from the noise probability density function to obtain the samples corresponding to the prior $p(x_k^i|y_{1:k-1})$ at time instant k.
- Update: The prediction is updated to get posterior $p(x_k^i|y_{1:k})$ at time step k using the current measurement by calculating likelihood for each sample as

$$p\left(y_k \middle| x_k^i\right) = e^{\left(-\frac{\left(y_k - h\left(x_k^i\right)^2\right)}{2R}\right)} \tag{3.36}$$

Higher the likelihood, higher is the probability of prediction being the current state based on current measurement only. Sometimes, after a few iterations the weights of most of the samples become negligible while the weights of rest of the few samples start to dominate. This phenomenon is called degeneracy and to avoid such situation the samples are resampled at every time instant. In resampling process, more samples with significant weight are redrawn from the sample pool and they replace the samples with the significant weights. The current estimate is given by the mean of the resampled posterior.

CHAPTER IV

SIMULATION STUDY

In practical applications of the fuel cell systems, the overall load fluctuates according to the power requirement of the various electrical appliances that draw power from the fuel cell systems. For example, in the vehicular applications of the fuel cell systems, the load current changes when the vehicle accelerates or decelerates. To simulate the effect of load changes, the system model is integrated after giving a step change in the current. The state vector which is to be estimated consists of partial pressure of the reactant gases and the temperature. The mathematical model discussed in the chapter II was used to simulate the "true" state vector and the calculated voltage is used as the measurement corrupted with random noise. These models are coded in Matlab environment. A tool box developed by Hartikainen [5] for unscented Kalman filtering is used.

The simulation was run for 4000 seconds by implementing step change in load. The current is stepped up from 0 A to 20 A. The corresponding stack voltage (35 cells in a stack) is shown in Figure 6.

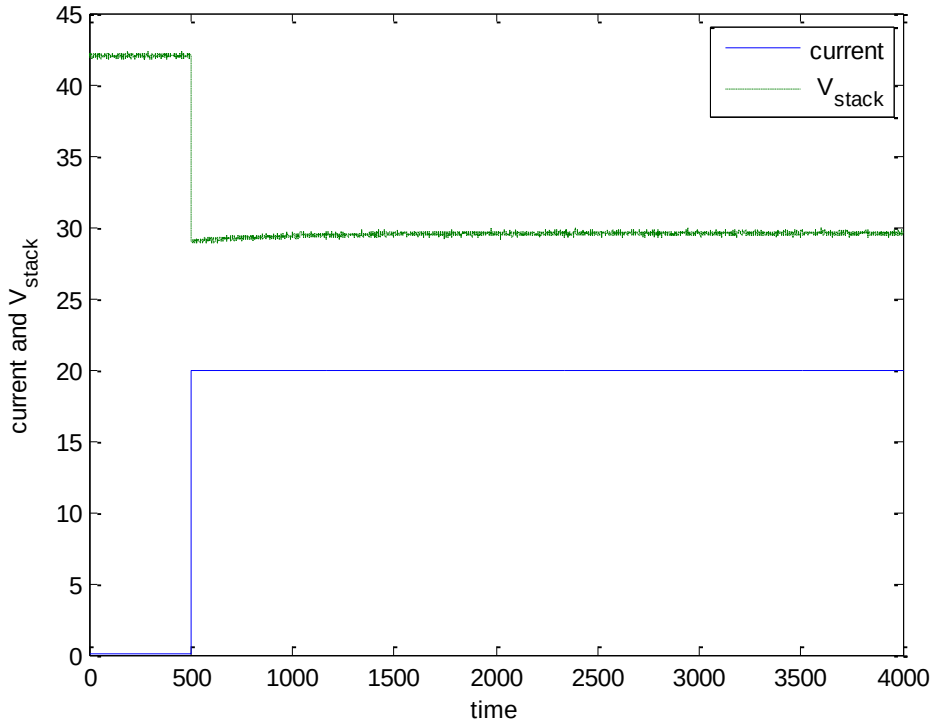

Figure 6: Step change in load

The system model is simulated with the initial conditions as

$$x_0 = [3.03 \;\; 3.375 \;\; 25.01]^T \tag{4.1}$$

and the filters are initialized with the initial estimates and prior covariance as

$$\hat{x}_0 = [3.03 \;\; 3.375 \;\; 25.01]^T$$
$$P_0 = \begin{bmatrix} 0.25^2 & 0 & 0 \\ 0 & 0.25^2 & 0 \\ 0 & 0 & 0.25^2 \end{bmatrix} \tag{4.2}$$

The system model used by the estimators is assumed to noisy. Therefore the filters are implemented with zero mean measurement noise with covariance R and zero mean process noise with covariance Q

$$R = 0.1^2$$
$$Q = \begin{bmatrix} 0.01^2 & 0 & 0 \\ 0 & 0.01^2 & 0 \\ 0 & 0 & 0.1^2 \end{bmatrix} \tag{4.3}$$

Number of samples taken for sequential Monte Carlo is 500. This chapter presents the simulation results for three cases.

- Good filter initialization
- Poor filter initialization
- Plant-model mismatch
- Multiple load changes

The performance of the filters is analyzed based on the mean square error which can be defined as

$$MSE = \frac{1}{N} \sum_{k=1}^{N} (x - \bar{x})^T (x - \bar{x}) \tag{4.3}$$

Where, N is the number of simulation points.

4.1 Good Filter Initialization

Following are simulation results, when both the filters are initialized with good initial estimates which are identical to the true initial condition. The estimates from sequential Monte Carlo (Figure 7) and unscented Kalman filter (Figure 8) are close to the true states with the mean squared error of 0.0387 and 0.036 respectively.

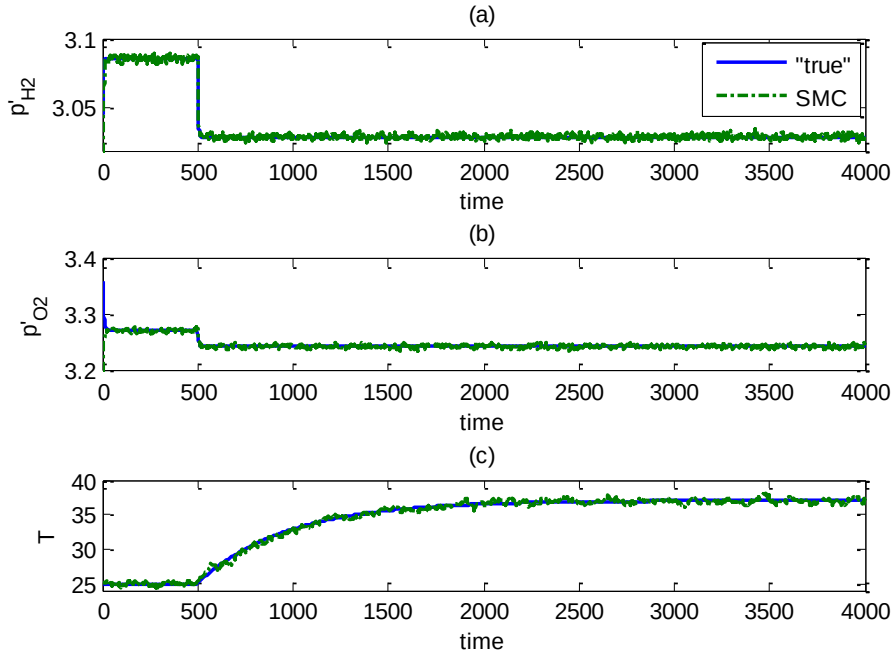

Figure 7: Estimates of p'_{H2}, p'_{O2} and T using SMC

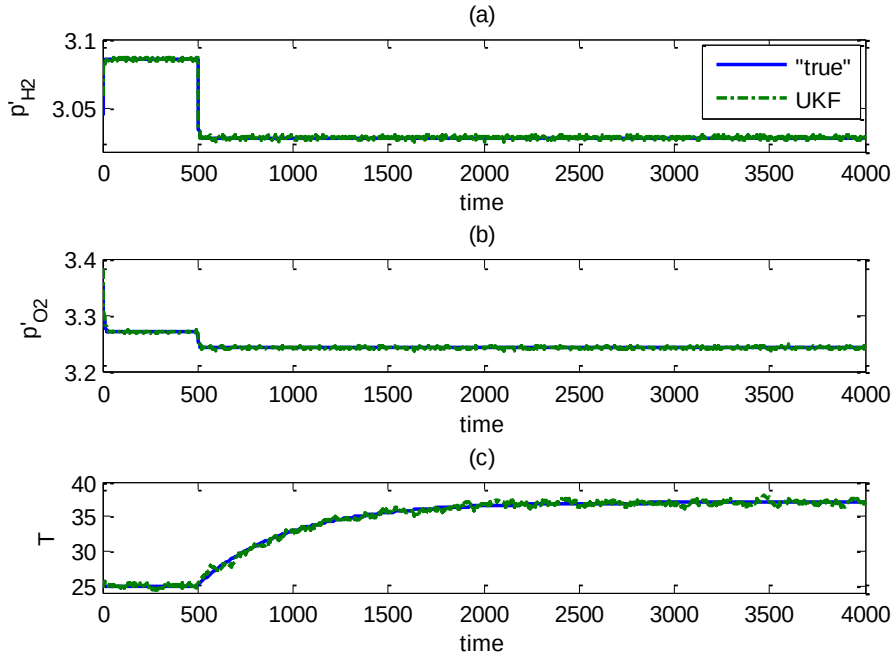

Figure 8: Estimates of p'_{H2}, p'_{O2} and T using UKF

Close up view of the estimate of partial pressure of hydrogen from unscented Kalman filter and sequential Monte Carlo restricted to first 50 seconds of simulation is shown in Figure 9. From this figure, it can be seen that the unscented Kalman filter converged to true state faster than sequential Monte Carlo. After converging to the true state, the estimates from both the filters are close to each other.

The closer view of estimates of partial pressure of oxygen and temperature from unscented Kalman filter and sequential Monte Carlo are show in Figure 10 and Figure 11 respectively. From these results it can be seen that the unscented Kalman filter converged to the true states faster than sequential Monte Carlo.

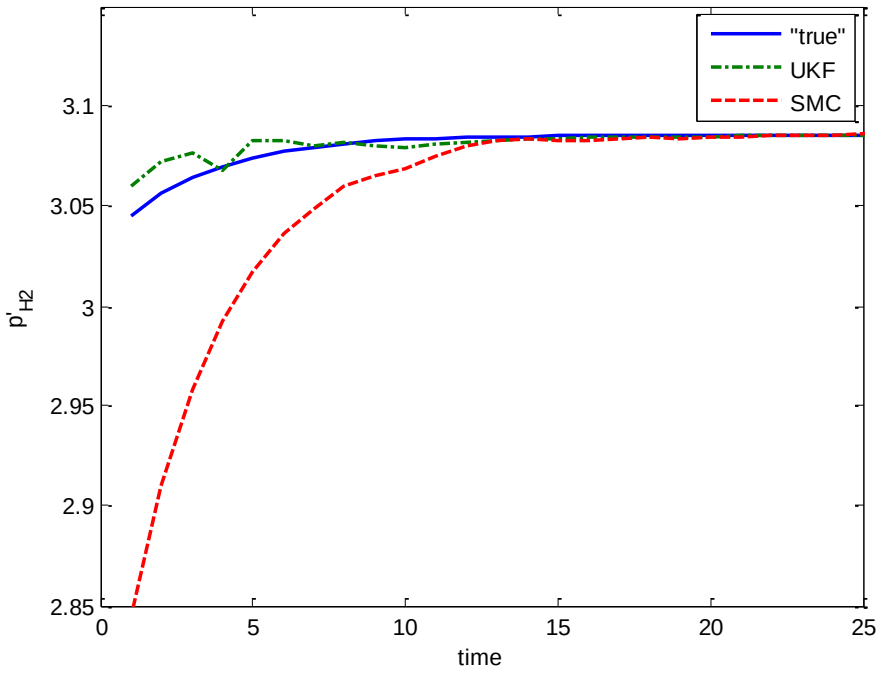

Figure 9: Zoomed in view from Figure 6(a) and Figure 7(a)

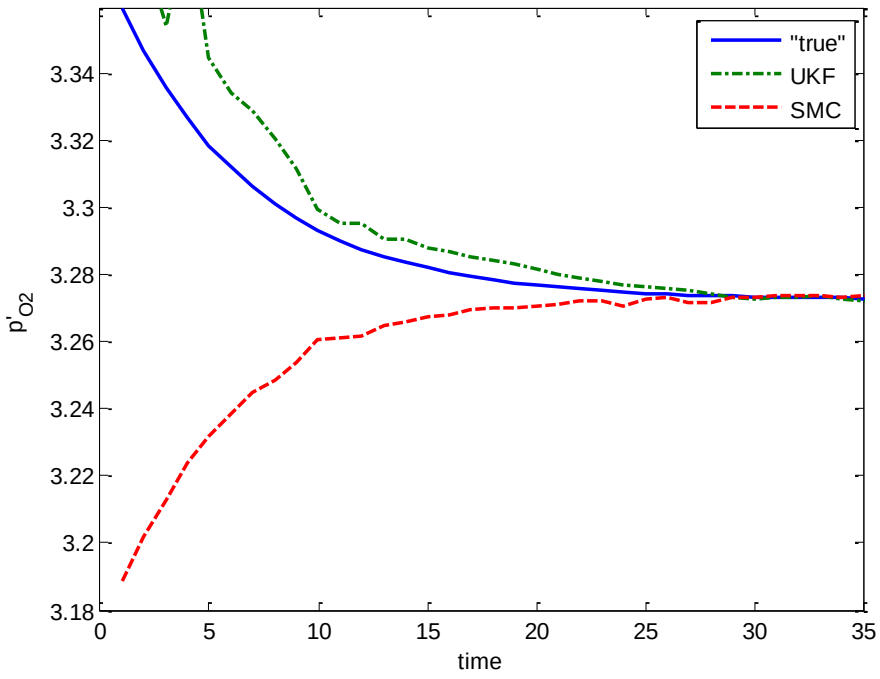

Figure 10: Zoomed in view of Figure 6(b) and Figure 7 (b)

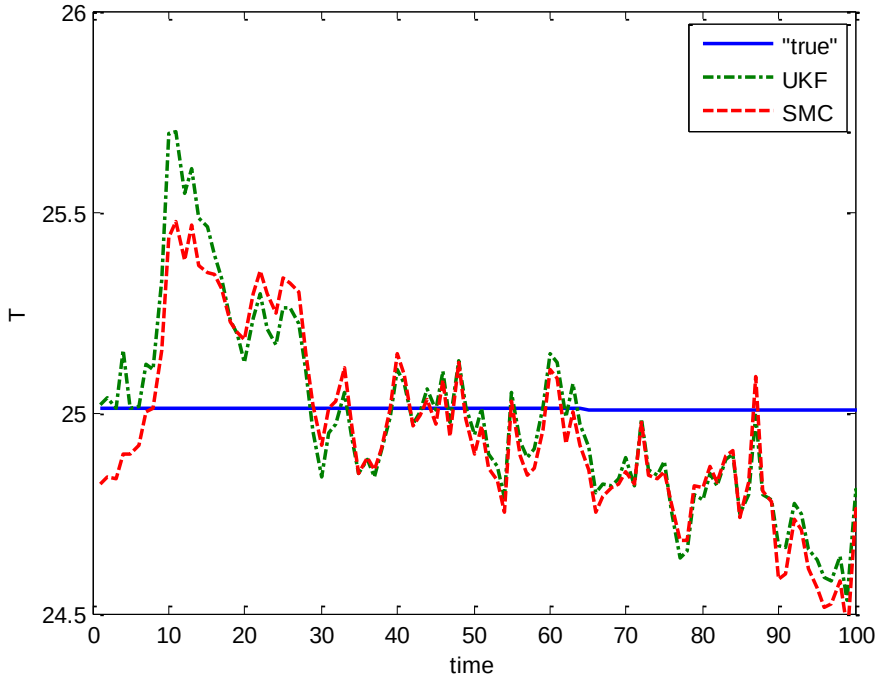

Figure 11: Zoomed in view from Figure 6(c) and Figure 7(c)

4.2 Poor filter initialization

The simulation was run by initializing the filters with poor initial estimates. Both the filters are initialized with the initial estimate and prior covariance as shown below.

$$xx = \begin{bmatrix} 5 & 1 & 25.01 \end{bmatrix}^T$$
$$P_0 = \begin{bmatrix} 0.005^2 & 0 & 0 \\ 0 & 0.005^2 & 0 \\ 0 & 0 & 0.005^2 \end{bmatrix} \tag{4.4}$$

Assuming the temperature can be initialized reasonably well, the initial estimate for temperature is not changed. Keeping the total pressure the same as the previous case, the initial estimates are taken as 5 atm and 1 atm for partial pressure of hydrogen and oxygen respectively. The prior covariance is reduced to simulate improper belief that the initial estimates are close to the true initial condition.

$$R = 0.1^2$$
$$Q = \begin{bmatrix} 0.01^2 & 0 & 0 \\ 0 & 0.01^2 & 0 \\ 0 & 0 & 0.1^2 \end{bmatrix} \tag{4.5}$$

Simulation results for the poor filter initialization are shown below. Estimates from sequential Monte Carlo (Figure 12) and unscented Kalman filter (Figure 13) converge to true states with the mean square error of 0.1991 and 0.0344 respectively.

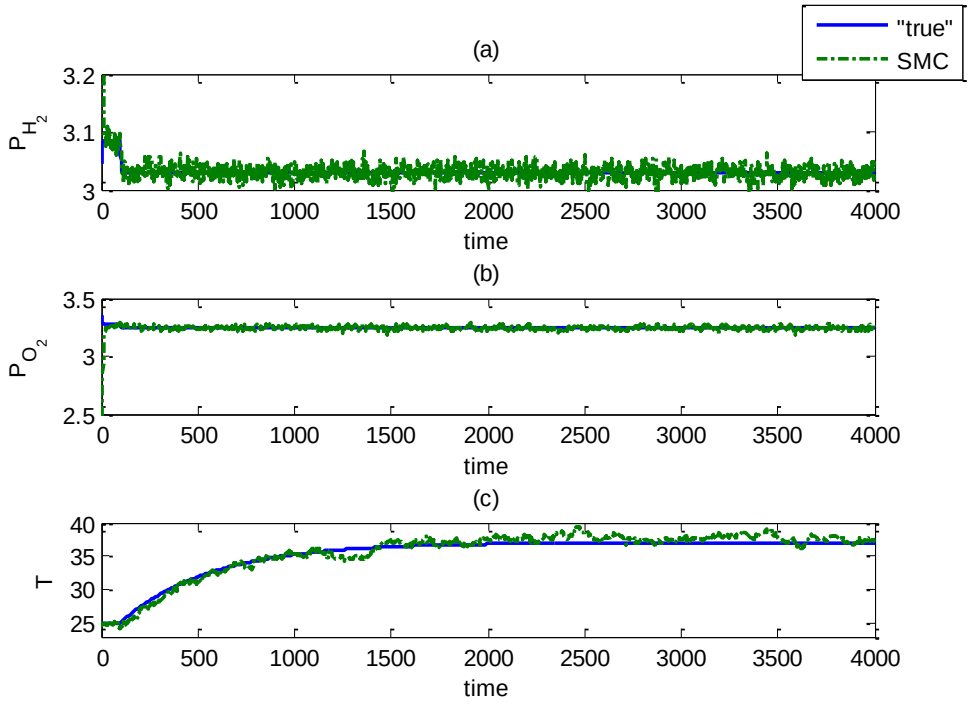

Figure 12: Estimates of p'_{H2}, p'_{O2} and T from SMC-Poor filter initialization

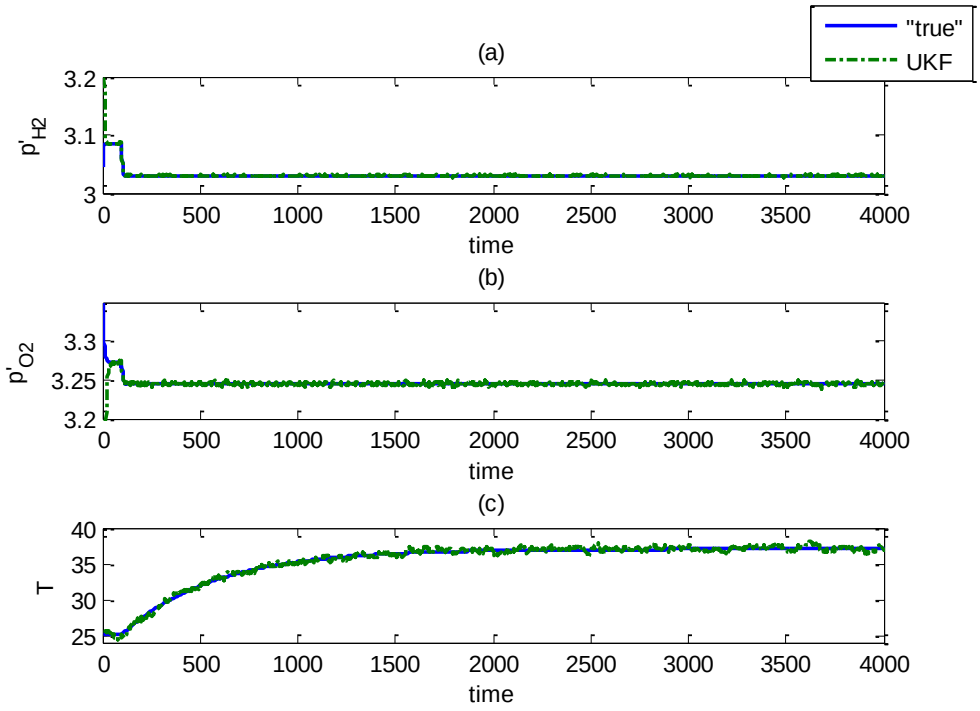

Figure 13: Estimates of p'_{H2}, p'_{O2} and T from UKF Poor filter initialization

Closer view of estimates of partial pressure of hydrogen and oxygen and temperature from unscented Kalman filter and sequential Monte Carlo are shown in Figure 14 and Figure 15 respectively. From these figures it can be seen that the estimates from both the filters converge at same time. The estimate of temperature (Figure 16) from the unscented Kalman filter converges to the true state (approximately 40 seconds) faster than the sequential Monte Carlo (approximately 10 seconds). Though the filters are initialized with poor initial estimates, they did not take much time to converge to the true initial condition. However, the estimates from the sequential Monte Carlo filter have more perturbations which led to high mean square error when compared to unscented Kalman filter.

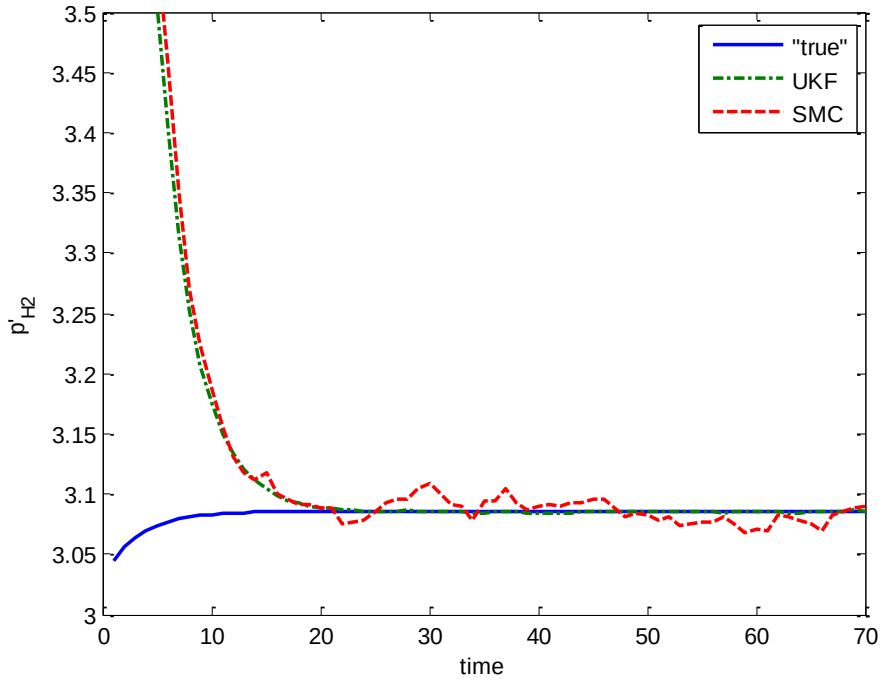

Figure 14: Zoomed in view from Figure 11(a) and Figure 12 (a)

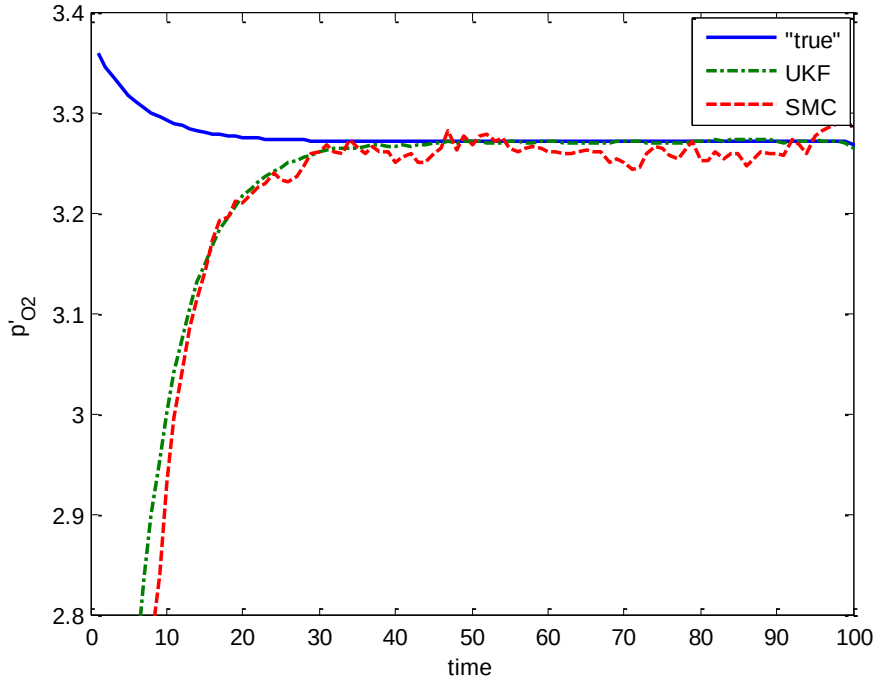

Figure 15: Zoomed in view of Figure 11(b) and Figure 12 (b)

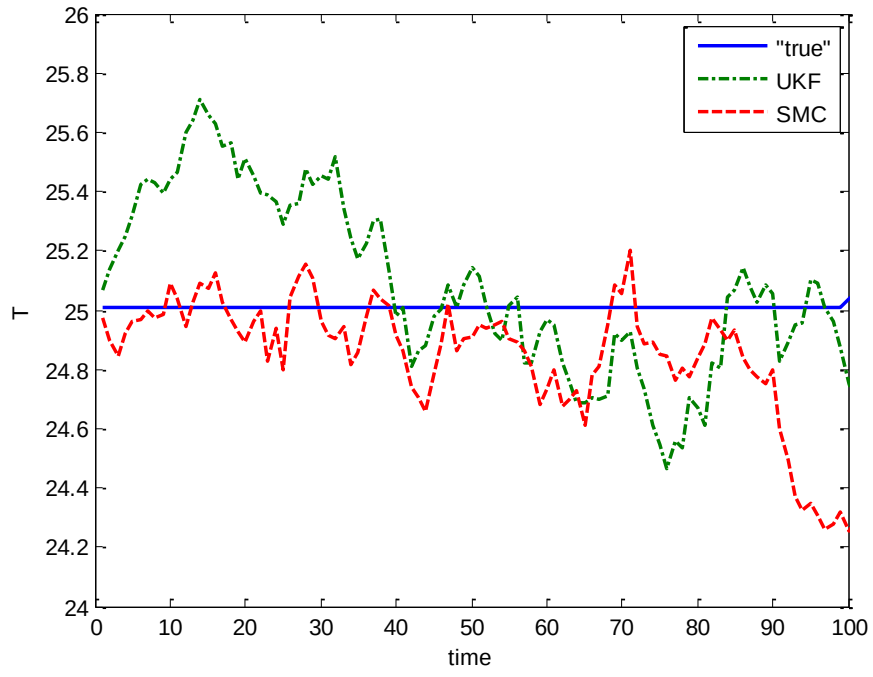

Figure 16: Zoomed in view of Figure 11(c) and Figure 12 (c)

4.3 Plant-Model Mismatch

The performance of the filters is studied when the system model used for the filters represents the true system with errors in some parameters. To study the performance, the simulation was run by introducing error in some of the parameters in the system model which is used for the filters. The parameters which are changed in the system model used for both filters are listed in Table II. ζ_1 and ζ_2 are parametric coefficients used in activation potential (equation 2.4) and A (equation 2.9) is cross sectional area. These parametric coefficients are determined experimentally and there is a possibility of presence of errors in these values. According the sensitivity analysis done by Corrêa [23] these parametric coefficients are sensitive and any error in these values have significant effect on the voltage term calculated from the electrochemical model. To simulate the effect of error prone values in the model used for filters, the selected parameters are introduced with 10% error in to the system model used for filters.

TABLE II: PARAMETERS USED IN THE PLANT-MODEL MISMATCH

Parameter	Value of parameter used in the "true" system model	Value of parameter used in plant-model mismatch
ζ_1	-0.948	-1.0428
ζ_4	$-1.93*10^{-4}$	$-2.123*10^{-4}$
A	232	255.2

The simulation results for the change in the value of the first parameter of the parametric form of activation potential (ζ_1) are shown below. The estimates converged to the true initial condition before implementing the step change. But after the step change, the

estimates from both sequential Monte Carlo (Figure 17) and unscented Kalman filter the filters (Figure 18) do not converge to the true states.

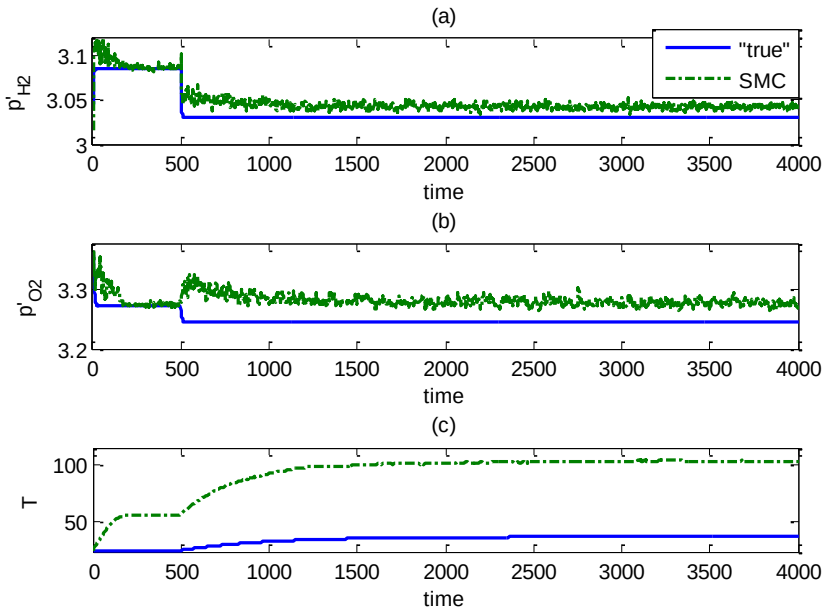

Figure 17: Estimates of p'_{H2}, p'_{O2} and T from SMC -plant-model mismatch

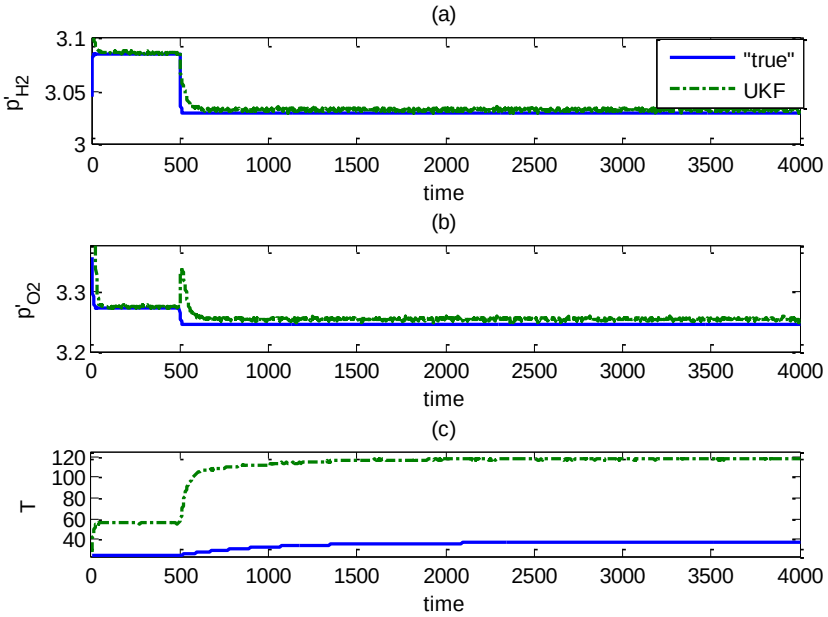

Figure 18: Estimates of p'_{H2}, p'_{O2}, and T from UKF- plant-model mismatch

The mean square error of the sequential Monte Carlo is 1202.872 where as the unscented Kalman filter has a mean square error of 1905.574. Following are the closer views of the estimates of partial pressure hydrogen from both the filters. From Figure19, it can be seen that the estimate of partial pressure of hydrogen from unscented Kalman filter converges to the true state faster than the sequential Monte Carlo filter. But after implementing the step change the estimate from the filters does not converge to the true state (Figure 20). The bias induced in the estimate of partial pressure of hydrogen is high for sequential Monte Carlo compared to unscented Kalman filter.

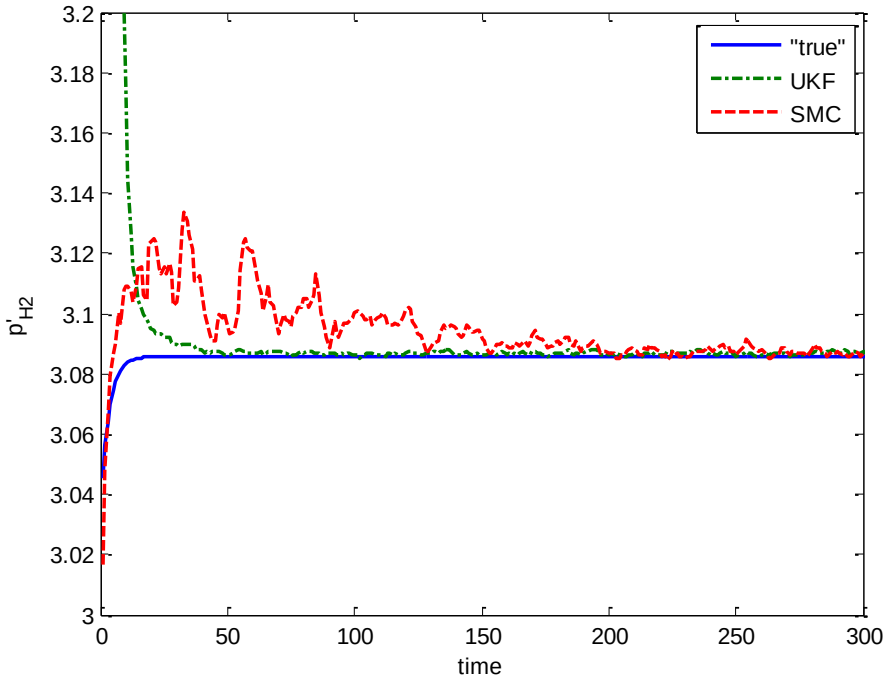

Figure19: Zoomed in view from Figure 17 (a) and Figure 18 (a) before step change

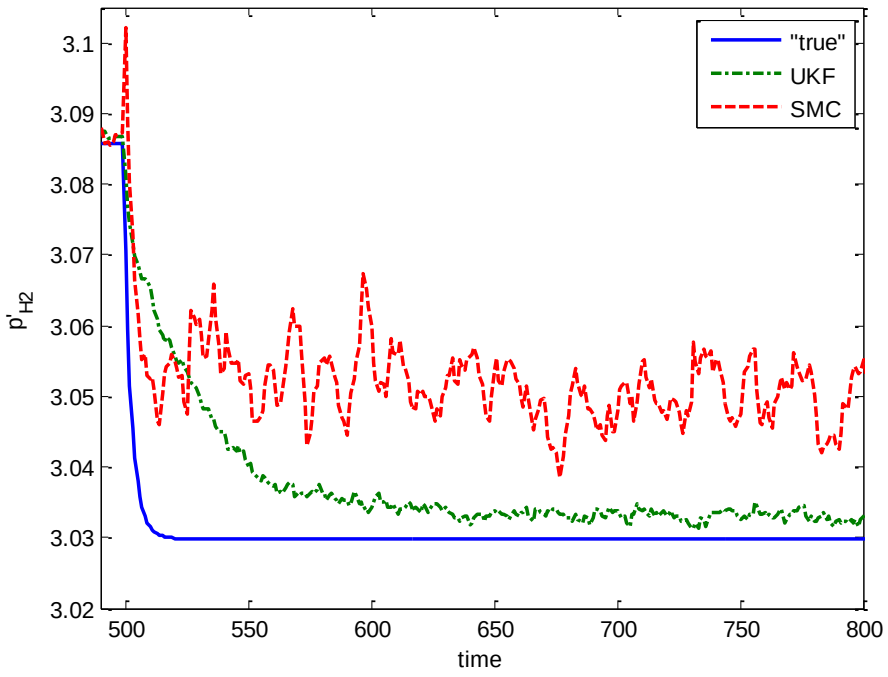

Figure 20: Zoomed in view from Figure 17 (a) and Figure 18 (a) after step change

Following are the closer view of estimate of partial pressure of oxygen from unscented Kalman filter and sequential Monte Carlo (Figure 21). The estimates from both the filters converge to the true state before the step change in load current is implemented. It can be seen that the estimate from sequential Monte Carlo takes longer time to converge to the true state when compared to unscented Kalman filters. However, the estimates did not converge to the true state after the implementation of step change (Figure 22). The estimate from the sequential Monte Carlo has larger bias than that of unscented Kalman filter.

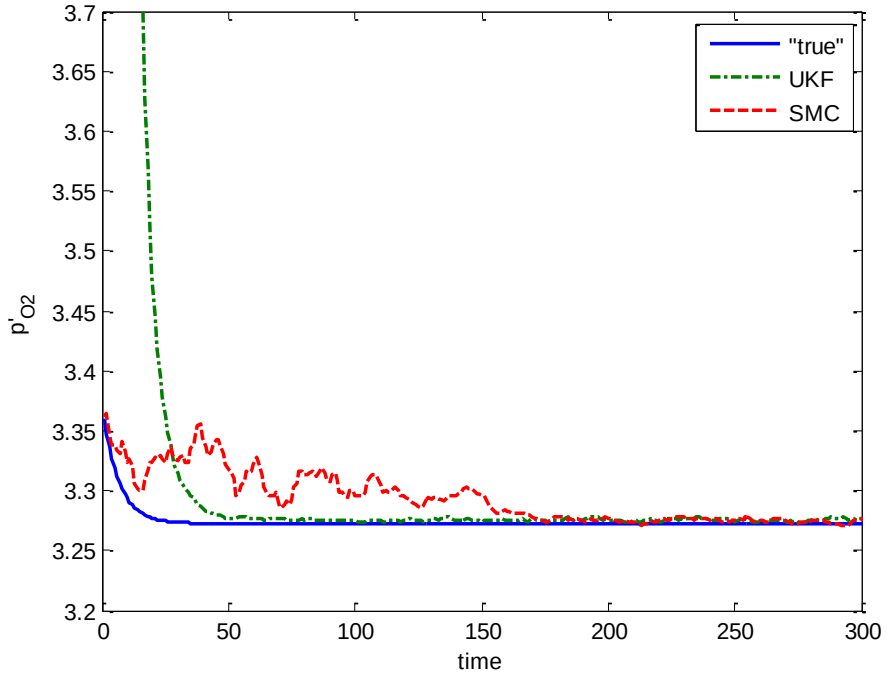

Figure 21: Closer view from Figureb17 (b) and Figure 18 (b) before step change

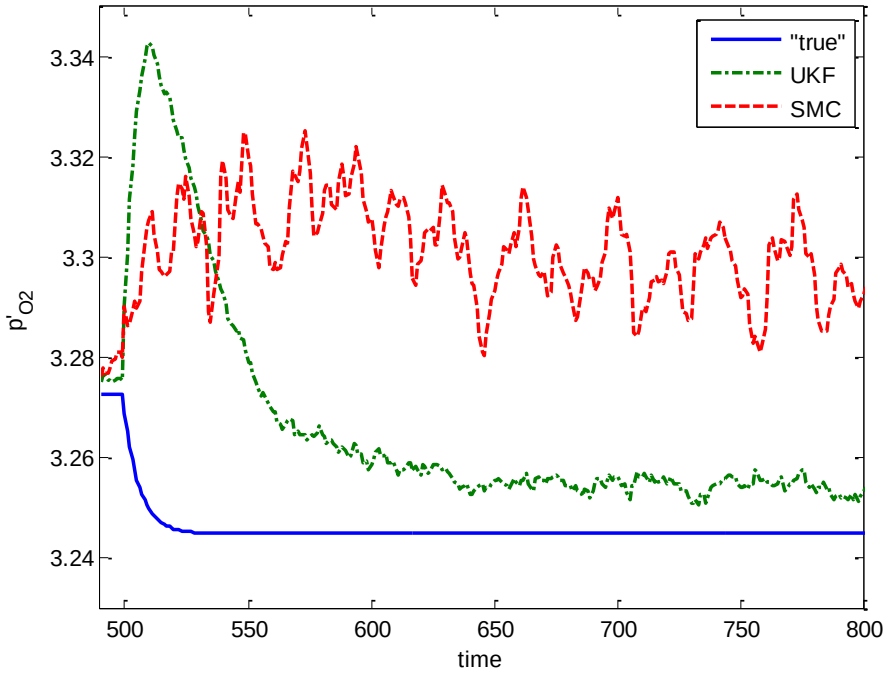

Figure 22: Closer view from Figureb17 (b) and Figure 18 (b) after step change

The estimate of temperature from unscented Kalman filter and sequential Monte Carlo is shown in Figure 23. From the figure it can be seen that the estimates did not converge to the true initial condition even before the implementation of the step change. There is bias induced in the estimate from both the filters and the temperature estimate goes up to 120^{o}C which cannot be seen in the practical applications. Unlike the estimates of partial pressure of the reactants, the bias induced in the estimates of temperature is high for the unscented Kalman filter compared to the sequential Monte Carlo and this accounts for the high mean square error.

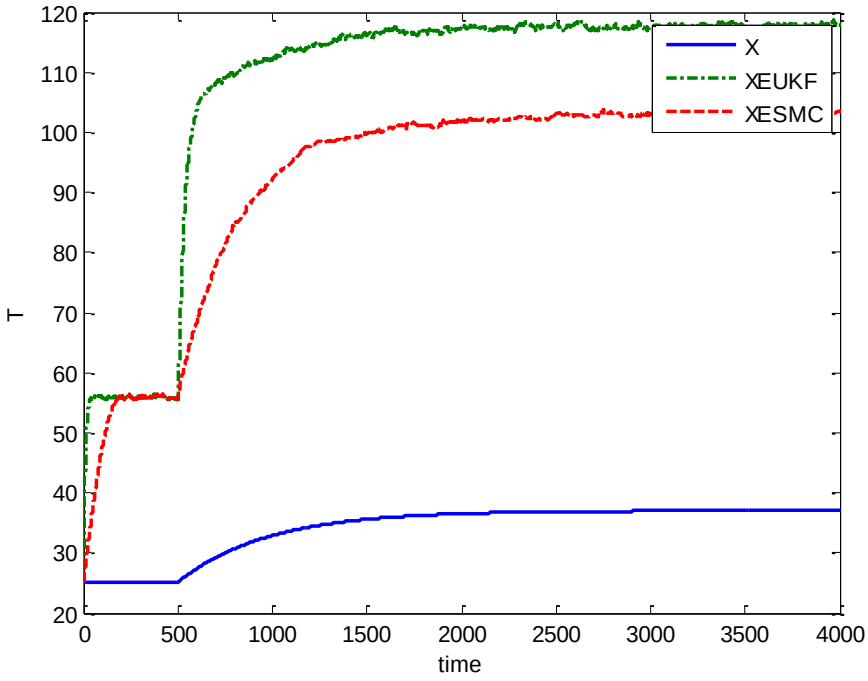

Figure 23: Temperature estimate from Figure 17 (c) and Figure 18 (c)

Figure 24 and Figure 25 show the simulation results for the change in fourth parametric coefficient ζ_4 in the activation potential. Unlike the estimates of partial pressure of hydrogen and oxygen, there is bias induced in the temperature estimate.

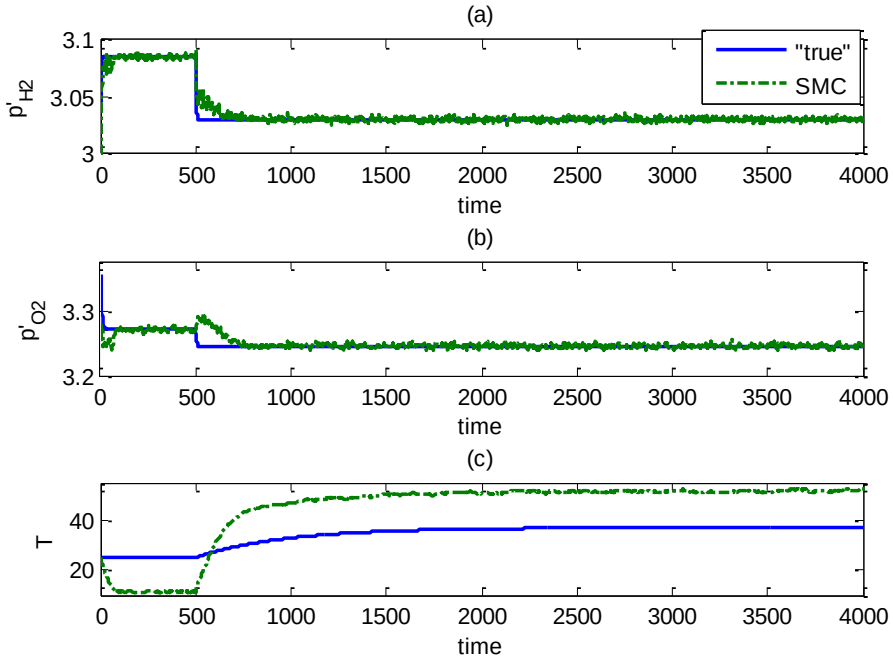

Figure 24: Estimates of p'_{H2}, p'_{O2}, and T from SMC-change in 4th parameter

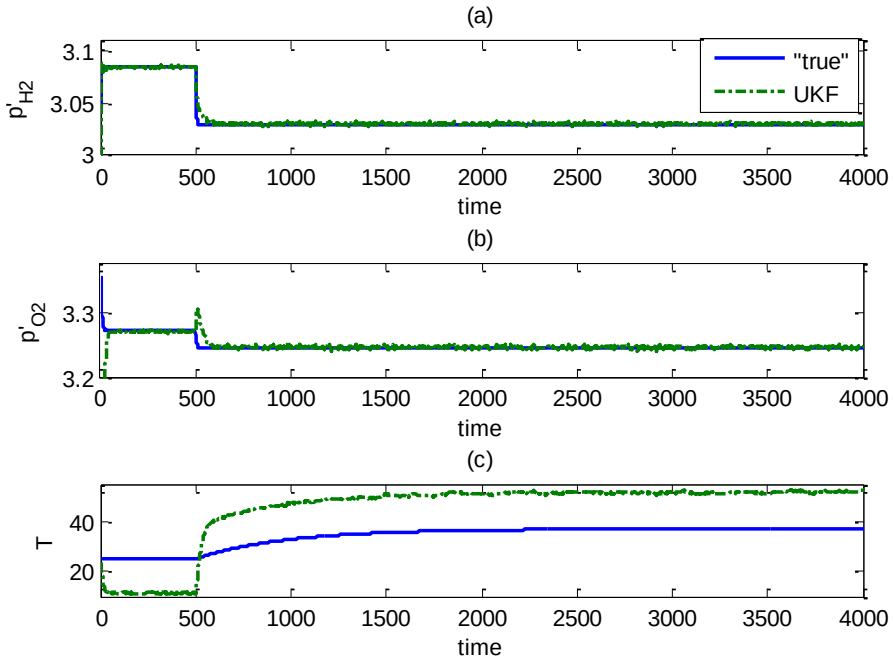

Figure 25: Estimates of p'_{H2}, p'_{O2} and T from UKF-change in 4th parameter

Hydrogen partial pressure estimate from both the filters after the implementation of step change is shown in Figure 26. It can be seen that the estimate from sequential Monte Carlo took long time to converge to the true state when compared to the unscented Kalman filter. Even after converging, the estimate has large perturbations compared to the estimate from unscented Kalman filter.

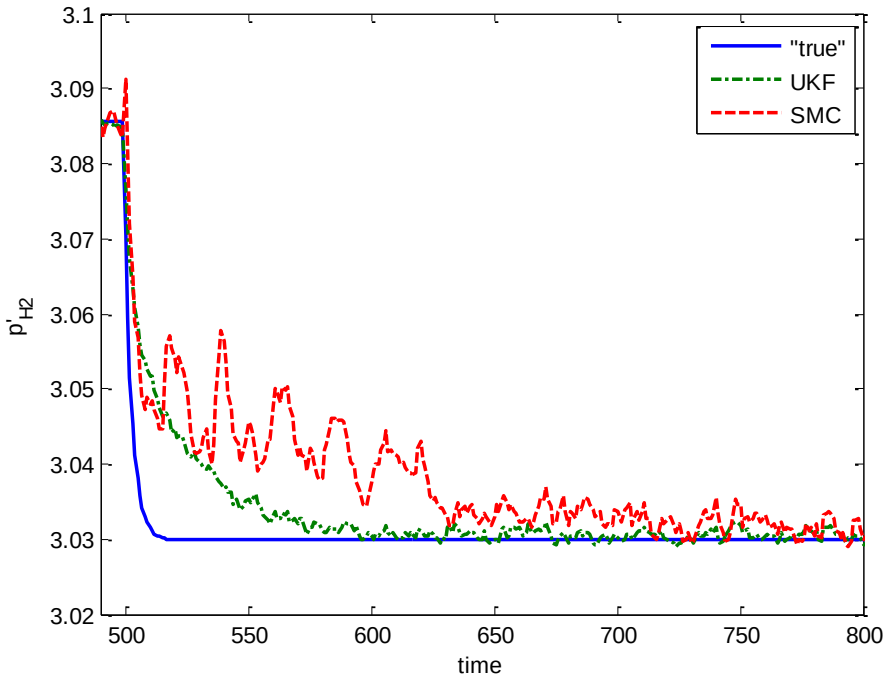

Figure 26: Zoomed in view from Figure 24 (a) and Figure 25 (a) after the step change

Figure 27 shows the estimate of oxygen partial pressure after the implementation of step change. It can be seen that the time taken to converge to the true state is larger for sequential Monte Carlo when compared to unscented Kalman filter.

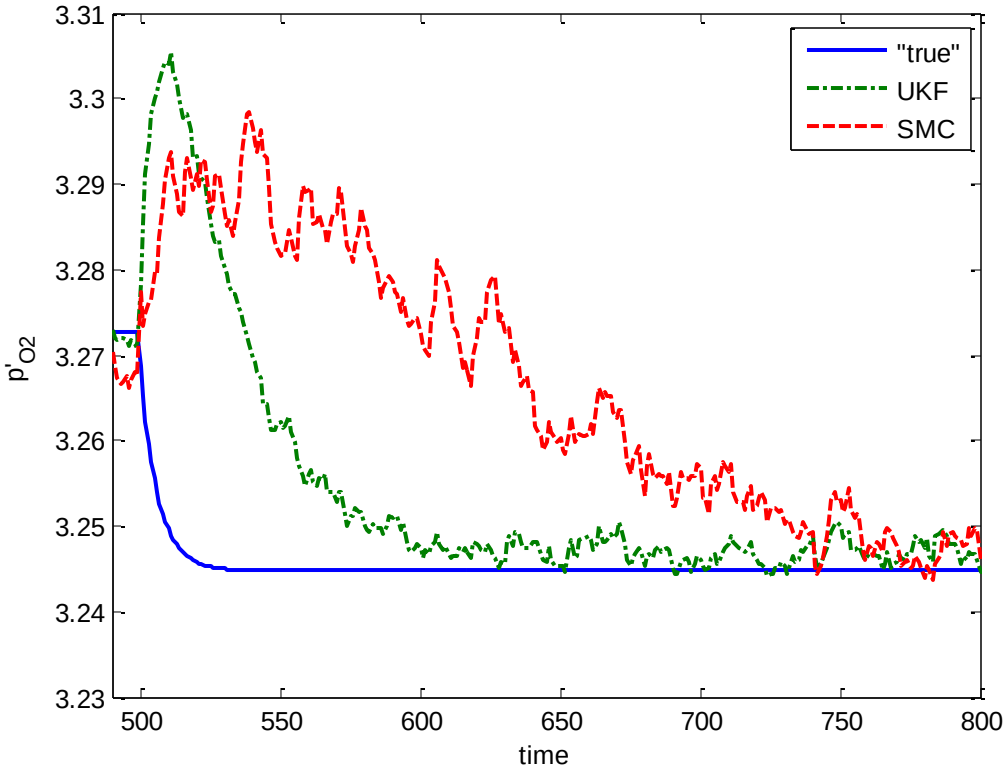

Figure 27: Zoomed in view of Figure.23 (b) and Figure.24 (b) after step change

The temperature estimate from both the unscented Kalman filter and sequential Monte Carlo is shown in Figure 28. The bias induced is approximately the same for both filters and the temperature estimate goes down to 10^{o}C (less than room temperature) which is not possible in the real time applications. Even though the estimates of partial pressure of hydrogen and oxygen from the unscented Kalman filter converge faster than the sequential Monte Carlo, it has higher mean square error (68.39) when compared to sequential Monte Carlo (65.38).

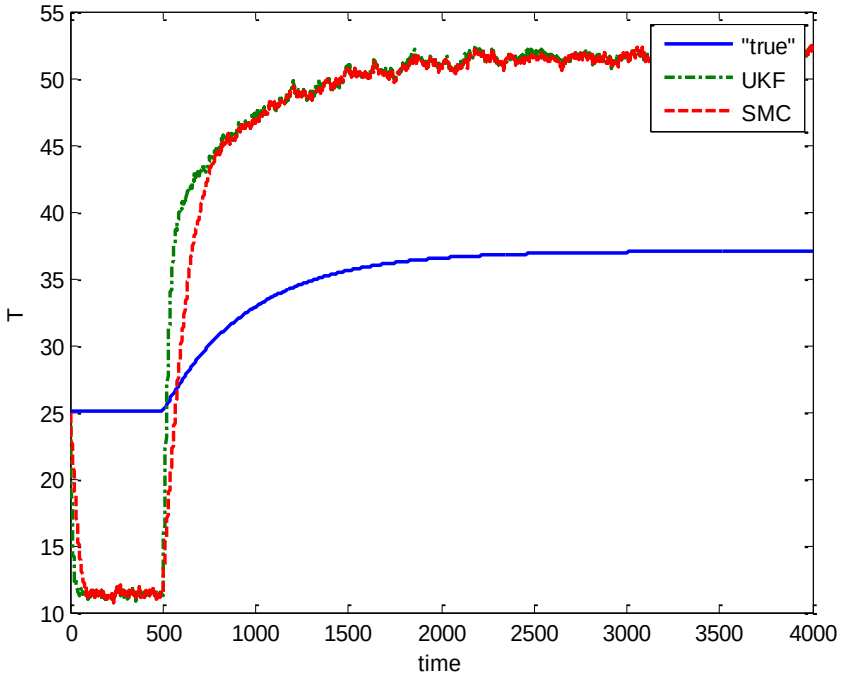

Figure 28: Temperature estimate from Figure 23 (c) and Figure 24 (c)

Following are the simulation results when the system model used for two filters is simulated by changing the value of active cell area (A). Form the Figure 29 and Figure 30, it can be seen that the estimates of partial pressure of the reactant gases from both the filters converge to the true states however the estimate for the temperature did not converge to the true state. The mean square error of unscented Kalman filter is 10.4475 and the mean square error of sequential Monte Carlo is 10.404.

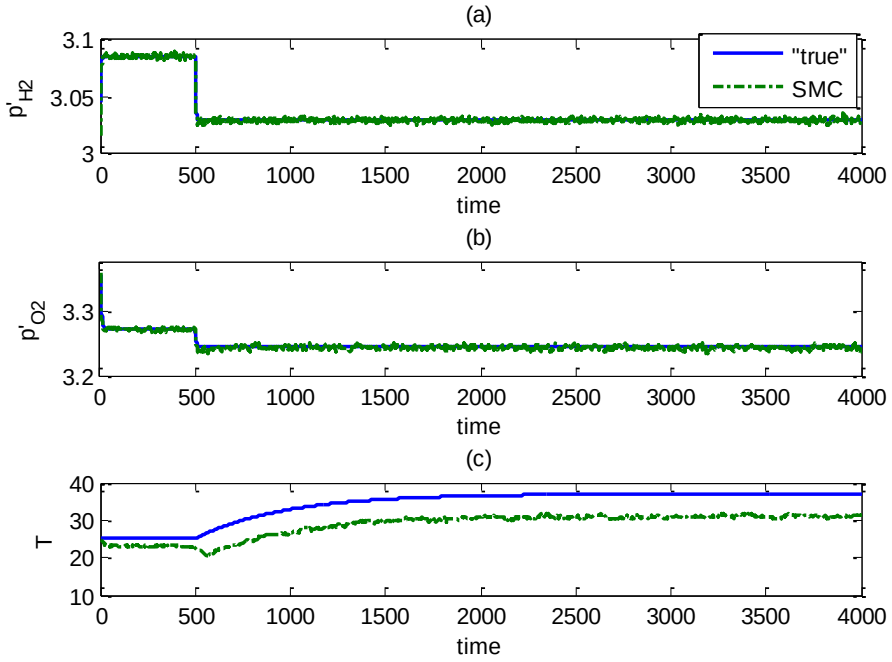

Figure 29: Estimates of p'_{H2}, p'_{O2}, and T from SMC-change in A

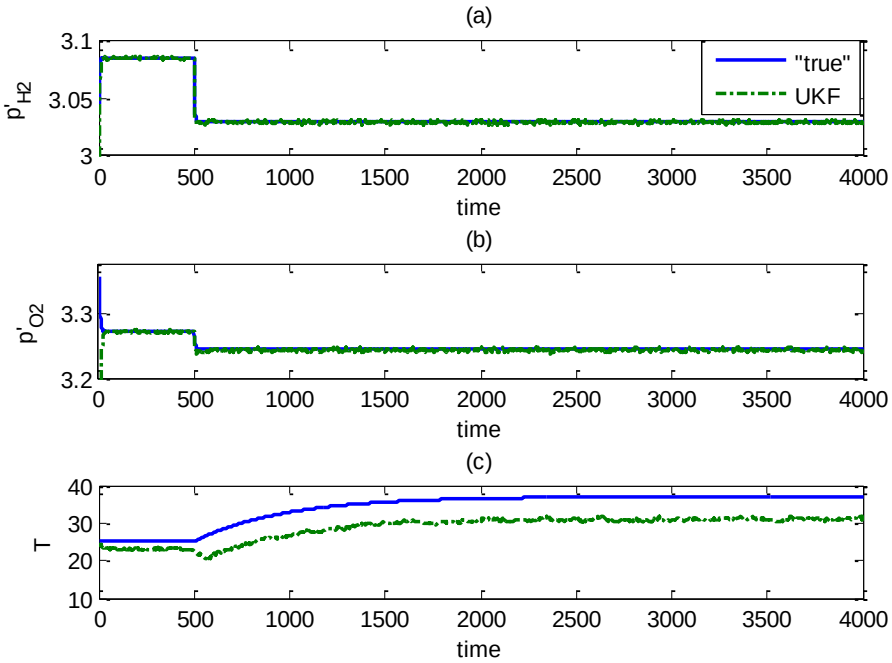

Figure 30: Estimates of p'_{H2}, p'_{O2}, and T from UKF-change A

Following are the zoomed in views of estimates of partial pressure of hydrogen and oxygen and temperature form both unscented Kalman filter and sequential Monte Carlo. The estimates of hydrogen partial pressure are shown in Figure 31. The hydrogen partial pressure estimate from the sequential Monte Carlo converges first compared to that of unscented Kalman filter. Figure 32 shows the oxygen partial pressure estimate. The partial pressure estimate form the sequential Monte Carlo converges first compared to the estimate from unscented Kalman filter. The temperature estimate from both the filters is shown in Figure 33. The bias induced in the temperature estimate from both the filters is same.

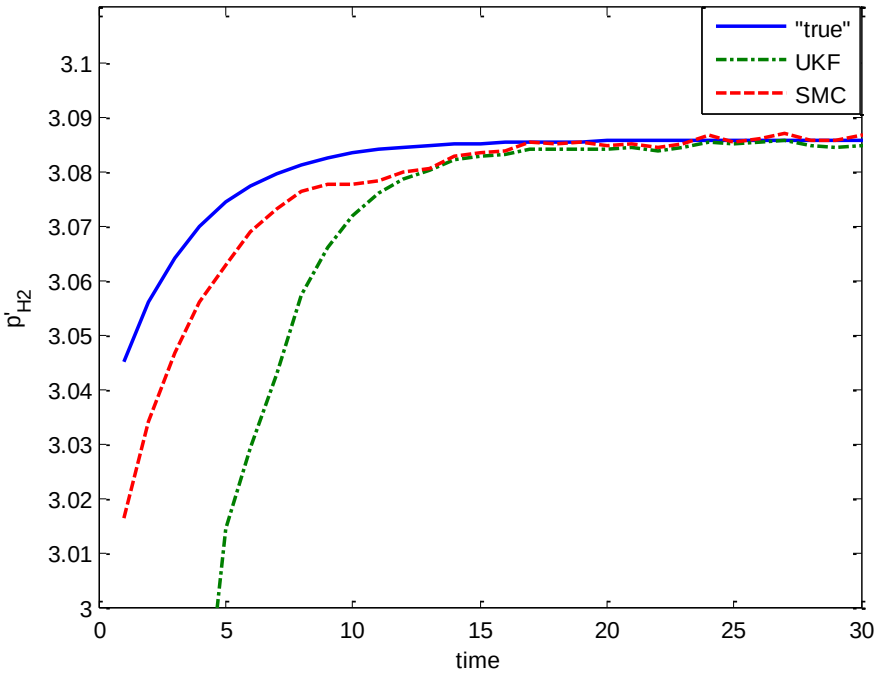

Figure 31: Zoomed in view from Figure 28 (a) and Figure 29 (a)

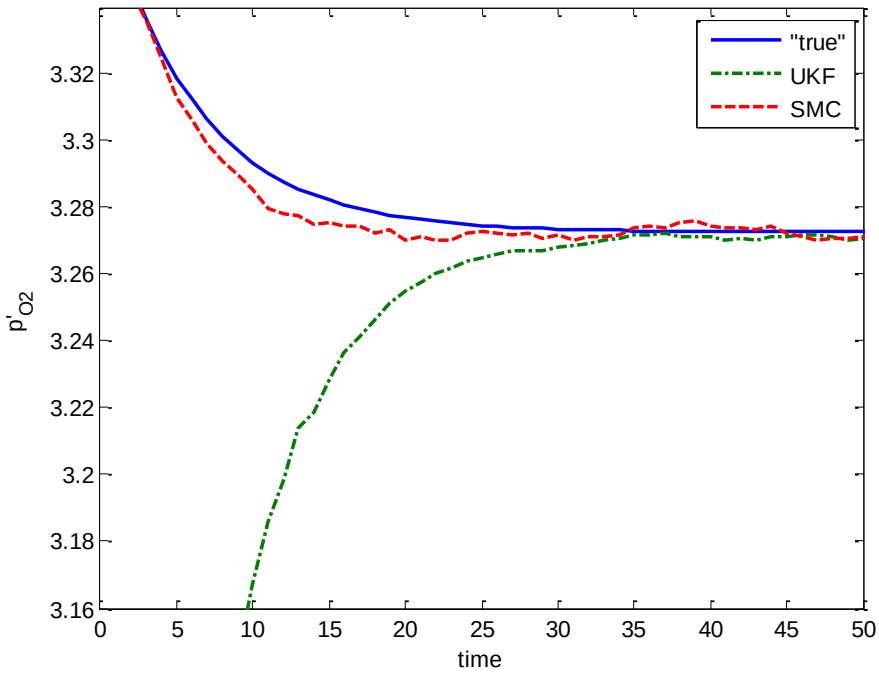

Figure 32: Zoomed in view from Figure 28 (b) and Figure 29 (b)

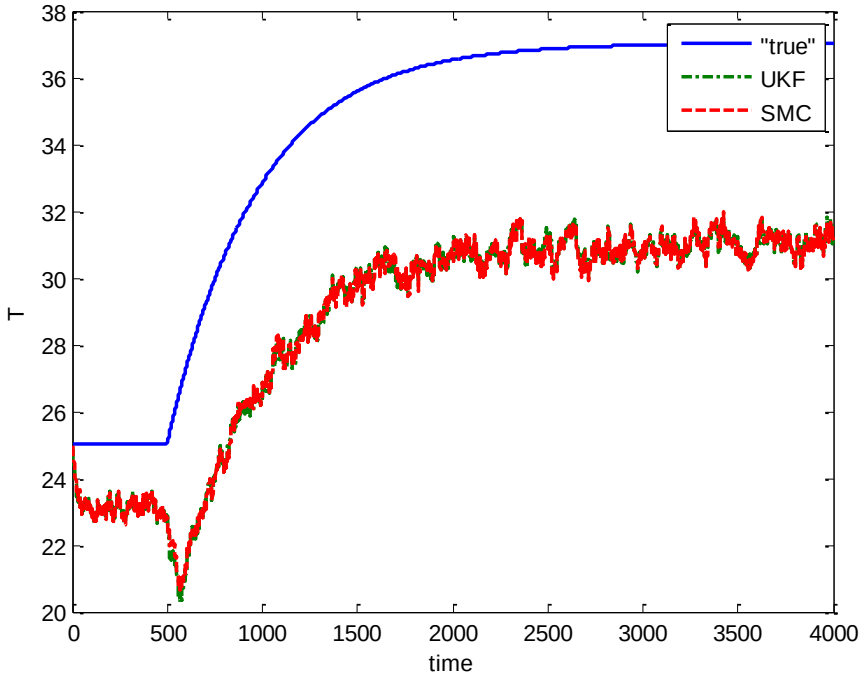

Figure 33: Temperature estimate from Figure 28 (c) and Figure 29 (c)

4.4 Multiple Load Changes

In vehicular applications, the load current changes according to the power requirement. To simulate the effect of multiple changes in the load, the system model is simulated by implementing multiple step change in the load current. The simulation was run for 10000 seconds. The filters were initialized with good initial estimates and with same process noise and measurement covariance as the above simulations. Following are the simulation results for the multiple load changes. From Figure 34 can be seen that as the load current changes, the output voltage fluctuates. Increase in the load current results in the increase in the fuel and oxidant consumption which in turn results in the decrease in the partial pressure of hydrogen and oxygen. The temperature of the stack also increases with the increases in the load current.

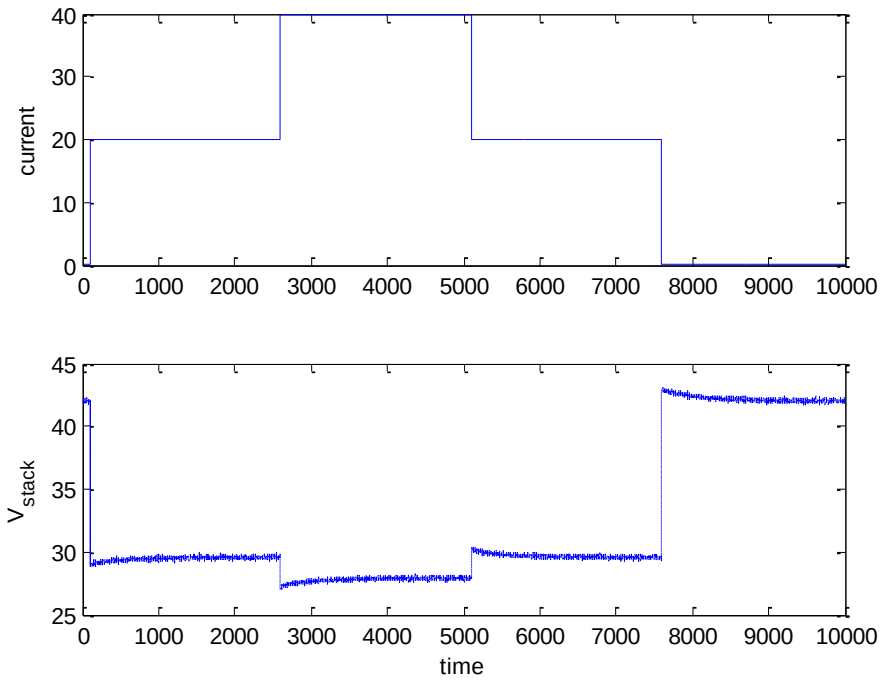

Figure 34: Current and voltage for multiple load changes

Below are the simulation results for the multiple variations in load. From these figures it can be seen that the estimates of hydrogen and oxygen partial pressure and temperature from sequential Monte Carlo [Figure 35] and unscented Kalman filter [Figure 36] are close to the true states with mean square error of 0.0331 for sequential Monte Carlo and 0.0313 for unscented Kalman filter.

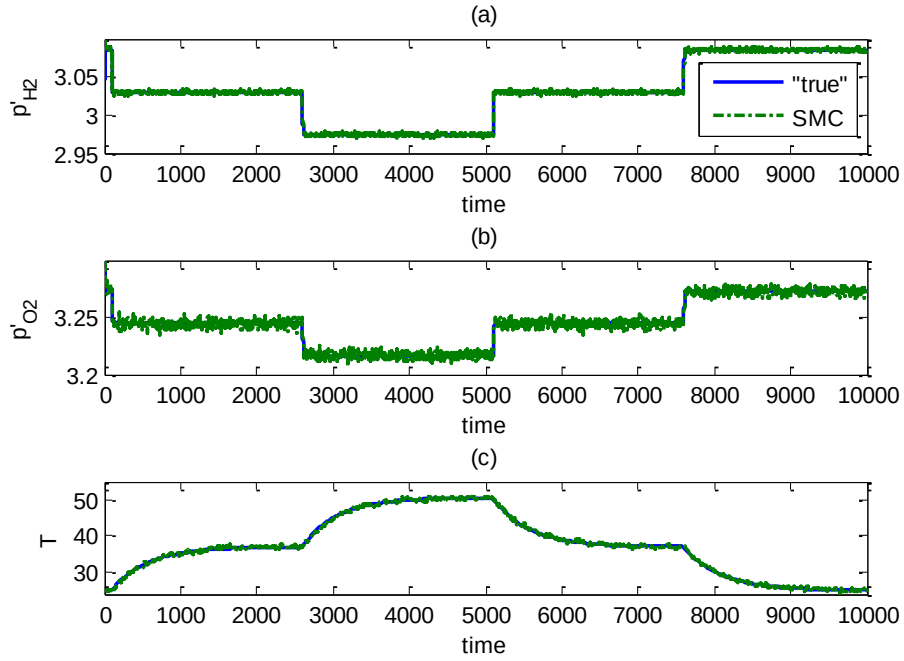

Figure 35: Estimates of p'_{H2}, p'_{O2} and T using SMC-multiple load changes

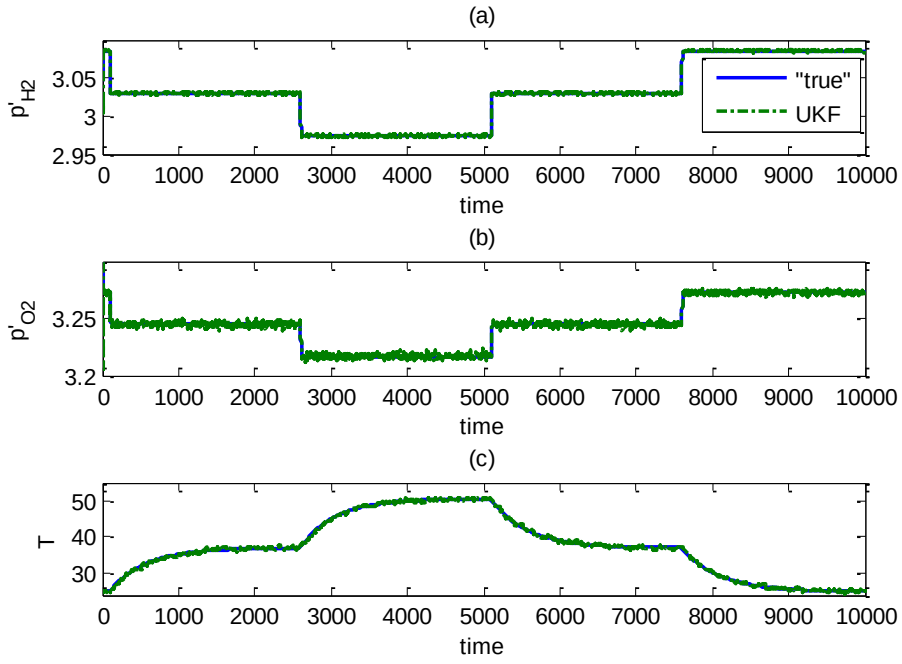

Figure 36: Estimates of p'_{H2}, p'_{O2} and T using UKF-multiple load changes

The mean square errors for both unscented Kalman filter and sequential Monte Carlo for above simulations are tabulated below (Table III). Tough the filters are initialized with poor initial estimates, the estimates from the both the filters converged quickly to the true initial condition. But, large mean square error of sequential Monte Carlo is due the presence of perturbations. The plant-model mismatch simulations were performed to see the influence of the error prone parameters of the system model. The parameters ζ_1 and ζ_3 have high influence on the model accuracy followed by the parameter ζ_4. This was also seen in the plant-model mismatch simulations. Change in the first parametric coefficient of the activation potential ζ_1 in the system resulted in a bias in the estimates with high mean square error. How ever the error is less for the change in the fourth parametric coefficient of the activation over potential ζ_4. According to the sensitivity analysis, the

cell active area (A) has no influence on the model accuracy; however, there is significant amount of bias induced in the temperature estimate from both the filters.

TABLE III: MSE FOR SMC AND UKF

SIMULATION	MSE_SMC	MSE_UKF
Good Filter Initialization	0.0387	0.036
Poor filter initial estimates	0.0372	0.0359
Plant model mismatch Change in ζ_1	1202.87	1905.574
Plant model mismatch Change in ζ_4	65.3807	68.3917
Plant model mismatch Change in Active cell area(A)	10.4475	10.404
Multiple load changes	0.0331	0.0313

The time taken for the simulation involving sequential Monte Carlo filter is about 6 hours and the time taken for simulation involving unscented Kalman filter is about 15 minutes. From the above table it can be seen that the unscented Kalman filter performance was much better than the sequential Monte Carlo filter and also it is computationally very efficient.

CHAPTER V

CONCLUSION AND FUTURE WORK

High efficiency, less emission of pollutants and reliability are key factors for the fuel cell technology to receive high research attention. Among the available fuel cells, polymer electrolyte membrane fuel cells received high attention for both stationary and mobile application because of its low operating temperature and relatively simple design.

In practical applications of fuel cell, the overall load fluctuates according to the power requirement. Increase in the load results in the increase in the consumption of fuel and oxidant which in turn results in the decrease in the partial pressure of reactants. The performance of the polymer electrolyte membrane fuel cell depends on membrane water content, partial pressure of fuel and oxidant and stack temperature and they must be properly controlled. High cost and the sensitivity of the sensors to the fluctuation in the gas composition limit the use of sensors in the practical applications. This motivates the need of estimator design.

The sequential Monte Carlo filter and unscented Kalman filter are applied to estimate the temperature and partial pressure of the reactant gases in polymer electrolyte membrane fuel cells. Generalized model proposed by Khan et al is used as system model for both

the filters. The performance of the filters is studied for three different cases, namely poor filter initialization, plant-model mismatch, multiple load variations. Even though the filters are initialized with the initial estimates which are far from the true initial conditions, both the filters converged to the true initial condition very quickly. But the estimates from sequential Monte Carlo filter have perturbations which led to high mean square error when compared to unscented Kalman filter. From the simulation results of plant-model mismatch, it can be seen that the estimates from both filters have bias which implies that the model used for the filters should be accurate.

Sequential Monte Carlo filter uses large number of samples to represent the probability density function of the states compared to unscented Kalman filter but still the estimates from the unscented Kalman filter are closer to the true states than the estimates from sequential Monte Carlo filter. This can be verified by calculating the mean square error. The mean square error of Sequential Monte Carlo filter is larger than that of unscented Kalman filter. The sequential Monte Carlo filter took 6 hours to complete where as the unscented Kalman filter took only 15 minutes to complete the simulation. Based on the computational time and mean square error, the performance of the unscented Kalman was better than the sequential Monte Carlo filter which is not anticipated.

Future Work

The control part is disused in this thesis and is left for the future work. The mathematical model that is used in this work is only for the fuel cell system. This model can be coupled

with the mathematical models of the auxiliary components such as fuel processor system, supply manifolds, compressors and humidifiers etc and the sequential Monte Carlo can be applied to estimate the parameters which are difficult to measure. These estimates can be used in control designs to increase the performance of the fuel cell stack.

REFERENCES

1. O'Hayre R, Cha S W, Colella W, Prinz F B, Fuel Cell Fundamentals, John Wiley & sons, inc, 2005
2. Grujicic M, Chittajallu K. M, Pukrushpan J. T, control of the transient behavior of polymer electrolyte membrane fuel cell systems, *proc. Institution of Mechanical Engineers Part D; J. Automobile Engineering*, 2004; 218: 1239-1250
3. McKay D, Stefanopoulou A G, Parameterization and validation of a lumped parameter diffusion model for fuel cell stack membrane humidity estimation, *proceedings of American control conferences,* 2004; 816-821.
4. Pukrushpan J T, Stefanopoulou A G, Peng H, Control of fuel cell power systems: principles, modeling, analysis and feedback design, Springer, Verlag London
5. Arcak M, Görgün H, Pedersen L M, Varigonda S, A nonlinear observer design for fuel cell hydrogen estimation, *IEEE Transactions on control systems technology,* 2004; 12: 101-110.
6. Görgün H, Arcak M, Barbir F, An algorithm for estimation of membrane water content in PEM fuel cells, *J. Power Sources*, 2006; 157: 389-394.
7. Carcadea E, Ene H, Ingham D B, Lazar R, Ma L, Puourkashanian M, Stefanescu I, Numerical simulation of mass charge transfer for PEM fuel cell, *International communications in heat and mass transfer*, 2005; 32: 1273-1280.
8. Springer T E, Zawodzinski T A, Gottesfeld S, Polymer electrolyte fuel cell model, *J. Electrochemical. Society*. 1991; 138: 2334-2342.

9. Rowe A, Li X, Mathematical modeling of proton exchange membrane fuel cells, J. *Power sources*, 2001; 102: 82-96.
10. Baschuk J J and Li X, Modeling of polymer electrolyte membrane fuel cell stacks based on hydraulic network approach, *International J. Energy Research*, 2004; 28: 697-724.
11. Amphlett J C, Baumert R M, Mann R F, Peppley B A, Roberge P R, Performance modeling of the Ballard mark IV solid polymer electrolyte fuel cell: mechanistic model development, *J. Electrochemical. Society*. 1995; 142: 1-8
12. Amphlett J C, Baumert R M, Mann R F, Peppley B A, Roberge P R, Performance modeling of the Ballard mark IV solid polymer electrolyte fuel cell: empirical model development, *J. Electrochemical. Society*. 1995; 142: 1-8
13. Amphlett J C, Mann R F, Peppley B A, Roberge, Rodrigues A, P R A model predicting transient responses of proton exchange membrane fuel cells, *J. Power sources*, 1996; 61: 183-188.
14. Mann R F, Amphlett J C, Hooper M A I, Jensen H M, Peppley B A, Roberge P R, Development and application of a generalized steady state electrochemical model for a PEM fuel cell, *J. Power Sources*, 2000; 86: 173-180.
15. Khan M J, Iqbal M T, Modeling and analysis of electrochemical and reactant flow dynamics for a PEM fuel cell system, *Fuel Cells*, 2005; 5: 463-475.
16. Huang B, Wang Q G, overview of emerging Bayesian approach to nonlinear system identification, *international workshop on solving industrial control and optimization problems*, 2006.

17. Kandepu R, Foss B, Imsland L, Applying the unscented Kalman filter for nonlinear state estimation, *J. Process Control,* 2008; 18: 753-768.
18. Julier S J, Uhlmann J K, Unscented Filtering and nonlinear estimation, *proceedings of the IEEE*, 2004; 92 : 401-422.
19. Simon J. Julier, Jeffrey K. Uhlmann, A new extension of the Kalman filter to nonlinear systems.
20. Ungarala S, Chen Z, Li K, Bayesian state estimation of nonlinear systems using approximate aggregate markov chains, *Industrial & Engineering Chemistry Research, 2006*; 45: 4208-4221.
21. Chen W S, Bakshi B R, Goel P R, Ungarala S, Bayesian estimation via sequential Monte Carlo sampling unconstrained nonlinear dynamic systems *Industrial & Engineering Chemistry Research, 2004*; 43: 4012-4025.
22. Lang L, Chen W S, Bakshi B R, Goel P R, Ungarala S, Bayesian estimation via sequential Monte Carlo sampling- Constrained dynamic systems, *Automatica*, 2007; 43: 1615-1622.
23. Corrêa J M, Farret F A, Popov V A, Simõs M G, Sensitivity analysis of the modeling parameters used in simulation of proton exchange membrane fuel cells, *IEEE transaction of energy conversion*, 2005; 20: 211-218.
24. Hartikainen J, Sarkka S, Matlab Toolbox Ekf/Ukf, 2008.

APPENDICES

```
%Constants and simulation parameters

N=35;                                          %no of cells in a
stack

R=8.314;                                           %gas constant
J/mol K

F=96485;                                       %Faraday constant
C/mol

A=232;                                         % area cm^2

lambda=12.5;                        % measure of water content(function
of membrane humidity)

lmem=178e-4;                    %membrane thickness cm

R1= 8.206e-5 ;                  %Gas constant m^3atm/mol K

moin=120*7.034e-4*0.21;         %inlet flow rate of oxygen mol/sec

mhin=8*7.03e-4*0.99;            %inlet flow rate of hydrogen mol/sec

Pbpr=3;                         %oxygen pressure outlet atm

kc=0.065;                       %cathode flow constant mol/sec atm

ka=0.065;                       %anode flow constant mol/sec atm

Ptank=3;                        %inlet hydrogen pressure atm

Va=0.005;                       %anode volume m^3

Vc=0.010;                       %cathode volume m^3

deltaH=285.5*1000;              %enthalpy J/mol
```

```
hcond=35.55;                    %H.E Conduction index W/oC(centigrade)

hconv=0.025;                    %H.E convection index W/C A

Tamb=25;                        %ambient temperature oC

Rt=0.115;                       %Thermal resistance oC/W

Ct=17.9*1000;                   %Thermal Capacitance J/oC

Tcwin=25;                       %inlet cooling water temperature oC

xi1=-0.948;                     %parametric coefficient

xi3=7.6e-5;                     %parametric coefficient

xi4=-1.93e-4;                   %parametric coefficient


% SIMULATION PARAMETERS

n=3;

Ndat=4000;                     %no of data poits

Q=[0.01^2 0 0;0 0.01^2 0;0 0 0.1^2];  %process noise coaviance

Nsamp=500;

cov=.1^2;                       %measurement noise covariance
```

Simulation for generating true states

```
%main file

global I

Ndat=4000;

n=3;

xx=[3.03 3.375 25.01 ]';

v_n=.1^2;

current=[ ];

Y=[ ];

X=[ ];

current=[ ];

for k=1:Ndat

 k

 if k<500

   I=0.05;

else

      I=20;

end


  x=simulation_data(xx);

    y=measurement_data(x);

    y=y+gauss_rnd(0,v_n,1);

    xx=x;
```

```
    X=[X x];
    Y=[Y y];
    current=[current I];
end
save X Y
t=[1:1:Ndat];
plot(t,current,t,Y);legend('current','voltage');xlabel('time');ylabel('
current voltage')
 subplot(311);plot(t,X(1,:));xlabel('time');ylabel('pH_2');
subplot(312);plot(t,X(2,:));xlabel('time');ylabel('pO_2');
subplot(313);plot(t,X(3,:));xlabel('time');ylabel('T');
```

Unscented Kalman filter

```
global I
f_func=@simulation_data;
h_func=@measurement_data;
Ndat=4000;
n=3;
dT=1;
M=[3.03 3.375 25.01]';
P=0.25^eye(3);
u_n=[0.01^2 0 0;0 0.01^2 0;0 0 0.1^2];
```

```
v_n=.1^2;
for k=1:size(Y,2)


 k
     if k<500
        I=0.05;
    else
        I=20;
     end
 [M,P]=ukf_predict1(M,P,f_func,u_n);
[M,P]=ukf_update1(M,P,Y(:,k),h_func,v_n);
XEUKF(:,k)=M;
pp_ukf1(:,:,k)=P ;
end
MSE_UKF1=sum(sum((X-XEUKF).^2))/Ndat/n
save MSE_UKF1 XEUKF
 % t=[1:1:Ndat];
subplot(311);plot(t,X(1,:),t,XEUKF(1,:));subplot(312);plot(t,X(2,:),t,X
EUKF(2,:));subplot(313);plot(t,X(3,:),t,XEUKF(3,:));
figure;
plot(t,X(1,:),'.',t,XEUKF(1,:));legend('X','XEUKF');xlabel('time');ylab
el('P_{H_2}')
figure;
```

```
plot(t,X(2,:),'.',t,XEUKF(2,:));legend('X','XEUKF');xlabel('time');ylab
el('P_{O_2}')

figure;

plot(t,X(3,:),'.',t,XEUKF(3,:));legend('X','XEUKF');xlabel('time');ylab
el('temperature')
```

Sequential Monte Carlo

```
%main file

global I

Ndat=4000;

%no of data poits

Nsamp=500;

%no of samples used.

n=3;

%no of states.

dT=1;

%length of time span

priormean=[3.03 3.375   25.01];

%mean of prior

priorcov=0.25^2*eye(3);

%covariance of prior

cov=.1^2;v_n=cov;

%measurement noise covariance
```

```
xprior=ones(Nsamp,n)*diag(priormean)+gauss_rnd(zeros(3,1),v_n,Nsamp)';

wbf_cputime=cputime;

XESMC=[ ];

Xpost=[ ];

Xprior=[xprior];

for k=1:Ndat

k

    if k<500

    I=0.05;

   else

      I=20;

   end


 [xhat      Xprior      xposterior
lkh]=filter_smc_estimate(Y(:,k),xprior);

xprior=Xprior;

XESMC=[XESMC  xhat'];

Xpost=[Xpost xposterior];

Xprior=[Xprior xprior];

end

 MSE_SMC = (sum(sum((X-XESMC).^2)'))/Ndat/n %finding mean square error

 wbf_cputime = cputime-wbf_cputime    %claculate the CPU time

 save MSE_SMC XESMC
```

```
t=[1:1:Ndat];

subplot(311);plot(t,X(1,:),t,XEUKF(1,:),t,XESMC(1,:));subplot(312);plot
(t,X(2,:),t,XEUKF(2,:),t,XESMC(2,:));subplot(313);plot(t,X(3,:),t,XEUKF
(3,:),t,XESMC(3,:));

figure

plot(t,X(1,:),t,XEUKF(1,:),'-.',t,XESMC(1,:),'--
','LineWidth',2);legend('X','XEUKF','XESMC');xlabel('time');ylabel('P_{
H_2}')

figure

plot(t,X(2,:),t,XEUKF(2,:),'-.',t,XESMC(2,:),'--
','LineWidth',2);legend('X','XEUKF','XESMC');xlabel('time');ylabel('P_{
O_2}')

figure

plot(t,X(3,:),t,XEUKF(3,:),'-.',t,XESMC(3,:),'--
','LineWidth',2);legend('X','XEUKF','XESMC');xlabel('time');ylabel('T')
subplot(311);plot(t,X(1,:),t,XEUKF(1,:),t,XESMC(1,:));xlabel('time');yl
abel('pH_2');

subplot(312);plot(t,X(2,:),t,XEUKF(2,:),t,XESMC(2,:));xlabel('time');yl
abel('pO_2');

subplot(313);plot(t,X(3,:),t,XEUKF(3,:),t,XESMC(3,:));xlabel('time');yl
abel('T');
```

Function File: for sequential Monte Carlo filter.

```
filter_smc_estimate

function [xhat Xprior xposterior lkh]=filter_smc_estimate(Y,xprior)

Nsamp=500;

Q=[0.01^2 0 0;0 0.01^2 0;0 0 0.1^2];

cov=.1^2;

n=3;

indx=zeros(1,Nsamp);

e1=Y-measurement_data_smc(xprior);

lkh = exp(-e1.^2/2/cov(1,1));

 lkh=lkh/sum(lkh);

%Resample form discrete distriubution

 distrib=cumsum(lkh);

      for j=1:Nsamp

        indx(j)=min(find((rand-distrib)<0));

      end

 xposterior=xprior(indx,:);

 xhat=mean( xposterior);%mean estimation

 [r,c]=size(xposterior);

  x0=reshape(xposterior,r*c,1);

 [t,pp]=ode23tb('system_equation_smc',[0 1],x0);

  kk=pp(size(pp,1),:);
```

```
  kk=reshape(pp(size(pp,1),:),length(pp(size(pp,1),:))/n,n);
  Xprior=kk+gauss_rnd(zeros(3,1),Q,Nsamp)';
```

Function File: Simulating the data

```
function xf=simulation_data(xx,dT)
dT=1;
[t yy]=ode23tb('system_equation',[0 dT],xx) ;
xf=yy(size(yy,1),:)';
```

Function File: Which has all the differential equations used in the model

```
function dx=system_equation(t,x)
global I
Constants
Ph=x(1,:);
Po=x(2,:);
T=x(3,:);
TK=T+273;
Tcwout=Tcwin+0.4*(T-Tcwin);
Ptot=N*I*deltaH/(2*F);
UAHX=hcond+(hconv*I);
```

```
moout=kc*(Po-Pbpr);

mhout=ka*(Ph-Ptank);

Qcool=UAHX.*((T-Tcwin)-(T-Tcwout))./log((T-Tcwin)./(T-Tcwout));

Qloss=(T-Tamb)/Rt;

ENernst=1.229-8.5e-4.*(TK-298.15)+R.*TK.*log(Ph.*(Po.^0.5))./(2*F);

Ch=Ph.*9.174e-7.*exp(-77./TK);

Co=Po.*1.97e-7.*exp(498./TK);

xi2=0.00286+0.0002*log(A)+4.3e-5*log(Ch);

Vact=xi1+xi2.*TK+xi3.*TK.*(log(Co))+xi4.*TK.*log(I);

rM=(181.6.*(1+0.03.*(I/A)+0.062.*(TK./303).^2.*(I/A).^2.5))./((lambda-
0.634-(3.*(I/A)))*exp(4.18.*(TK-303)./TK));

Rint=rM.*(lmem/A);

Vohmic=I.*Rint;

V=ENernst+Vact-Vohmic;

Vstack=V*N;

Pelec=Vstack*I;



dx=[R1.*TK.*(mhin-mhout-N*I/(2*F))./Va;

    R1.*TK.*(moin-moout-N*I/(4*F))./Vc;

    (Ptot-Pelec-Qcool-Qloss)./Ct];
```

Function File: which gives the measurements

```
function y_n=measurement_data(x,param)
```

```
global I

Constants

Ph=x(1,:);

Po=x(2,:);

T=x(3,:);

TK=T+273;

Tcwout=Tcwin+0.4*(T-Tcwin);

ENernst=1.229-8.5e-4.*(TK-298.15)+R.*TK.*log(Ph.*(Po.^0.5))./(2*F);

Ch=Ph.*9.174e-7.*exp(-77./TK);

Co=Po.*1.97e-7.*exp(498./TK);

xi2=0.00286+0.0002*log(A)+4.3e-5*log(Ch);

Vact=xi1+xi2.*TK+xi3.*TK.*(log(Co))+xi4.*TK.*log(I);

rM=(181.6.*(1+0.03.*(I/A)+0.062.*(TK./303).^2.*(I/A).^2.5))./((lambda-
0.634-(3.*(I/A)))*exp(4.18.*(TK-303)./TK));

Rint=rM*lmem/A;

Vohmic=I*Rint;

V=ENernst+Vact-Vohmic;

y_n=V*N;
```

Function File: which has all the differential equations used in the model. This file is used for SMC.

```
function dx=system_equation_smc(t,x)
```

```
global I

Constants

x=reshape(x,length(x)/n,n);

Ph=x(:,1);

Po=x(:,2);

T=x(:,3);

TK=T+273;

Tcwout=Tcwin+0.4*(T-Tcwin);

Ptot=N*I*deltaH/(2*F);

UAHX=hcond+(hconv*I);

moout=kc*(Po-Pbpr);

mhout=ka*(Ph-Ptank);

Qcool=UAHX.*((T-Tcwin)-(T-Tcwout))./log((T-Tcwin)./(T-Tcwout));

Qloss=(T-Tamb)/Rt;

ENernst=1.229-8.5e-4.*(TK-298.15)+R.*TK.*log(Ph.*(Po.^0.5))./(2*F);

Ch=Ph.*9.174e-7.*exp(-77./TK);

Co=Po.*1.97e-7.*exp(498./TK);

xi2=0.00286+0.0002*log(A)+4.3e-5*log(Ch);

Vact=xi1+xi2.*TK+xi3.*TK.*(log(Co))+xi4.*TK.*log(I);

rM=(181.6.*(1+0.03.*(I/A)+0.062.*(TK./303).^2.*(I/A).^2.5))./((lambda-
0.634-(3.*(I/A)))*exp(4.18.*(TK-303)./TK));

Rint=rM.*(lmem/A);

Vohmic=I.*Rint;
```

```
V=ENernst+Vact-Vohmic;

Vstack=V*N;

Pelec=Vstack*I;

dx=[R1.*TK.*(mhin-mhout-N*I/(2*F))./Va;

R1.*TK.*(moin-moout-N*I/(4*F))./Vc;

    (Ptot-Pelec-Qcool-Qloss)./Ct];
```

Function File: It gives the measurement . This is used for SMC which can incorporate the samples

```
function y_n=measurement_data_smc(x,param)

global I

Constants

Ph=x(:,1);

Po=x(:,2);

T=x(:,3);

TK=T+273;

Tcwout=Tcwin+0.4*(T-Tcwin);

ENernst=1.229-8.5e-4.*(TK-298.15)+R.*TK.*log(Ph.*(Po.^0.5))./(2*F);

Ch=Ph.*9.174e-7.*exp(-77./TK);

Co=Po.*1.97e-7.*exp(498./TK);

xi2=0.00286+0.0002*log(A)+4.3e-5*log(Ch);

Vact=xi1+xi2.*TK+xi3.*TK.*(log(Co))+xi4.*TK.*log(I);
```

```
rM=(181.6.*(1+0.03.*(I/A)+0.062.*(TK./303).^2.*(I/A).^2.5))./((lambda-
0.634-(3.*(I/A)))*exp(4.18.*(TK-303)./TK));

Rint=rM*lmem/A ;

Vohmic=I*Rint;

V=ENernst+Vact-Vohmic;
```

y_n=V*N;